Iron insertion at the assembly site of the ISCU scaffold protein is a conserved process initiating Fe–S cluster biosynthesis

Batoul Srour, Sylvain Gervason, Maren Hellen Hoock, Beata Monfort, Kristian Want, Djabir Larkem, Nadine Trabelsi, Gautier Landrot, Andrea Zitolo, Emiliano Fonda, et al.

Iron insertion at the assembly site of the ISCU scaffold protein is a conserved process initiating Fe-S cluster biosynthesis

Batoul Srour,[1±] Sylvain Gervason,[1±] Maren Hellen Hoock,[4] Beata Monfort,[1] Kristian Want,[1] Djabir Larkem,[1] Nadine Trabelsi,[1] Gautier Landrot,[2] Andrea Zitolo,[2] Emiliano Fonda,[2] Emilien Etienne,[3] Guillaume Gerbaud,[3] Christina Sophia Müller,[4] Jonathan Oltmanns,[4] Jesse B. Gordon,[5] Vishal Yadav,[5] Malgorzata Kleczewska,[6] Marcin Jelen,[6] Michel B. Toledano,[1] Rafal Dutkiewicz,[6] David P. Goldberg,[5] Volker Schünemann,[4] Bruno Guigliarelli,[3] Bénédicte Burlat,[3] Christina Sizun,[7] Benoit D'Autréaux[1]*

[1] Université Paris-Saclay, CEA, CNRS, Institute for Integrative Biology of the Cell (I2BC), 91198, Gif-sur-Yvette, France

[2] Synchrotron SOLEIL, L'Orme des Merisiers, BP48 Saint Aubin 91192, Gif-Sur-Yvette, France

[3] Aix Marseille Univ, CNRS, Laboratoire de Bioénergétique et Ingénierie des Protéines (BIP), 31 chemin Joseph Aiguier 13402, Marseille, France

[4] Fachbereich Physik, Technische Universität Kaiserslautern, Erwin-Schrödinger-Str. 56, 67663 Kaiserslautern, Germany

[5] Department of Chemistry, The Johns Hopkins University, 3400 N. Charles Street, Baltimore, MD 21218, USA

[6] Intercollegiate Faculty of Biotechnology, University of Gdansk and Medical University of Gdansk, Abrahama 58, 80-307 Gdansk, Poland

[7] Institut de Chimie des Substances Naturelles, CNRS, Université Paris Saclay, avenue de la terrasse 91190 Gif-sur-Yvette, France

[±] These authors equally contributed

*Email: benoit.dautreaux@i2bc.paris-saclay.fr

Abstract

Iron-sulfur (Fe-S) clusters are prosthetic groups of proteins biosynthesized on scaffold proteins by highly conserved multi-protein machineries. Fe-S clusters biosynthesis into the ISCU scaffold protein is initiated by ferrous iron insertion followed by sulfur acquisition, via a still elusive mechanism. Notably, whether iron initially binds to the ISCU cysteine-rich assembly site or to a cysteine-less auxiliary site via N/O ligands remains unclear. We show here by SEC, CD and Mössbauer spectroscopies that iron binds to the assembly site of the monomeric form of prokaryotic and eukaryotic ISCU proteins via either one or two cysteines, referred to the 1-Cys and 2-Cys forms. The latter predominated at pH 8.0 and correlated with Fe-S cluster assembly activity, whereas the former increased at a more acidic pH, together with free iron, suggesting that it constitutes an intermediate of the iron insertion process. Iron not binding to the assembly site was non-specifically bound to aggregated ISCU, ruling out the existence of a structurally defined auxiliary site in ISCU. Characterization of the 2-Cys form by site-directed mutagenesis, CD, NMR, XAS, Mössbauer and EPR spectroscopies showed that the iron center is coordinated by four strictly conserved amino acids of the assembly site: Cys35, Asp37, Cys61 and His103 in a tetrahedral geometry. The sulfur receptor Cys104 was at very close distance and apparently bound to the iron center when His103 was missing, which may enable iron-dependent sulfur acquisition. Altogether, these data provide the structural basis to elucidate the Fe-S cluster assembly process and establish that the initiation of Fe-S cluster biosynthesis by insertion of a ferrous iron in the assembly site of ISCU is a conserved mechanism.

Introduction

Iron-sulfur (Fe-S) clusters are ubiquitous prosthetic groups of proteins made of iron and sulfide (S^{2-}) ions. Fe-S clusters are present in organisms from the three life-kingdoms (archaea, prokaryotes and eukaryotes), where they perform essential biological functions including ATP production, the Krebs cycle, the synthesis of proteins, DNA and several metabolites, nitrogen fixation and the maintenance of genome integrity.[1] The most common Fe-S clusters are the generic [2Fe2S] and [4Fe4S] clusters, but more complex Fe-S clusters are found in enzymes such as nitrogenase and hybrid cluster protein. The building block for all Fe-S clusters is the [2Fe2S] cluster that is biosynthesized *de novo* by multi-protein machineries orchestrating a complex multi-step process to assemble iron and sulfur ions in a proper and secured way. Three main machineries have been identified: the ISC (Iron Sulfur Cluster), the SUF (Sulfur mobilization) and the NIF (Nitrogen Fixation) machineries.[2-5] The ISC and SUF machineries are general providers of Fe-S clusters, while the NIF machinery is dedicated to assembling the Fe-S cluster of nitrogenase.[3,4] The ISC pathway is widespread across eukaryotes and proteobacteria and the SUF pathway is predominant in most bacteria, archaea and plants.[2,6-10] The ISC and SUF machineries of eukaryotes were inherited from a bacterial and archaeal ancestor, thus making these pathways share high homologies.[6,7,9]

Recent works have shed new light on the mechanism of Fe-S cluster assembly by the ISC machinery (**scheme 1**).[1,11-15] In eukaryotes this machinery encompasses a core complex made of the scaffold protein ISCU, the NFS1-ISD11-ACP complex containing the cysteine desulfurase NFS1, a pyridoxal-phosphate (PLP) enzyme providing sulfur to ISCU in the form of a cysteine-bound persulfide (Cys-SSH) by desulfurization of L-cysteine, and the ferredoxin 2 (FDX2) with its cognate reductase (FDXR) that together deliver electrons to reduce the persulfide. The assembly process is initiated by the insertion of a ferrous iron into ISCU (**scheme 1**, step 1), which triggers the transfer of a persulfide from NFS1 to ISCU (**scheme 1**, step 4).[12] FDX2-FDXR then reduces the persulfide into sulfide, which generates a [2Fe2S] cluster by a still ill-defined mechanism that may involve dimerization of ISCU (**scheme 1**, step 5).[11,12] Persulfide transfer and reduction were both shown to require the presence of iron in ISCU to synchronize sulfur insertion with iron availability in ISCU.[12] The whole process is stimulated by the frataxin protein (FXN) that accelerates Fe-S cluster assembly by accelerating persulfide transfer from NFS1 to ISCU (**scheme 1**, step 4).[12,14,15]

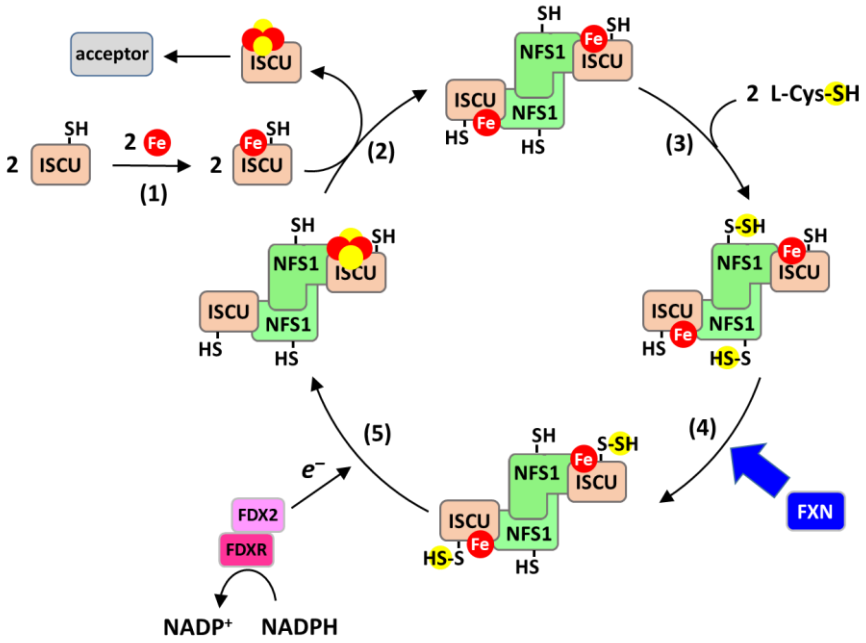

Scheme 1: Model of Fe-S cluster biosynthesis by the eukaryotic ISC machinery.
(**1**) iron binds to apo-ISCU generating Fe-ISCU, (**2**) two Fe-ISCU bind to the $(NFS1\text{-}ISD11\text{-}ACP)_2$ complex (ISD11 and ACP have been omitted for clarity) by exchange with holo-ISCU containing a [2Fe2S] cluster and apo-ISCU, (**3**) within the $(NFS1\text{-}ISD11\text{-}ACP\text{-}Fe\text{-}ISCU)_2$ complex, NFS1 reacts with L-cysteine, which generates a persulfide on the catalytic cysteines of both NFS1 subunits, (**4**) the persulfides on NFS1 are transferred to the Fe-ISCU subunits via a trans-persulfuration reaction and FXN accelerates this step, (**5**) FDX2/FDXR reduces the persulfide on Fe-ISCU into sulfide, which ultimately leads to the formation of a [2Fe2S] cluster, possibly via dimerization of ISCU.

Although the overall picture of the sequence of Fe-S cluster assembly is becoming clearer, the underlying mechanisms are still unclear; especially the coordination of the iron center at each stage of the assembly process. The assembly site of ISCU contains five strictly conserved amino acids that are essential for Fe-S cluster biogenesis *in vivo*: Cys35, Asp37, Cys61, His103 and Cys104 (in mouse ISCU numbering).[16-19] The strict conservation of these residues suggests that the assembly mechanism is also conserved across species.[20,21] Cys104 was identified as the persulfide receptor in mouse ISCU,[12,14] and the [2Fe2S] cluster is ultimately ligated by Cys35, Asp37, Cys61 and Cys104 at the last stage of the assembly process.[22-27] However, few data on the coordination changes at the assembly site occurring during the reaction process have been reported. Most available data were obtained from ISCU proteins containing zinc instead of iron (hereafter referred to as Zn-ISCU).[28,29] Although zinc can functionally replace iron to enable persulfide transfer and its acceleration by FXN (**scheme 1**, step 4),[12,13] structures of iron-containing ISCU proteins are missing to elucidate the mechanism of assembly. Different coordination arrangements were reported for the zinc ion at the early stages of the assembly process. In mouse Zn-ISCU (PDB code 1WFZ), the zinc ion appeared coordinated by Cys35, Asp37, Cys61 and His103, while Asp37 was free and Cys104 was a ligand in *Haemophilus influenzae* Zn-ISCU (PDB code 1RP9).[30] In *Escherichia coli* IscU, alanine substitutions of Asp39 or His105 retained their ability to bind zinc, suggesting that several configurations might be in equilibrium.[31] In human Zn-ISCU complexed

with NFS1-ISD11-ACP (PDB code 5WGB), the coordination of the zinc center was similar to mouse Zn-ISCU, except that Cys35 was exchanged with the catalytic cysteine of NFS1, most likely to allow persulfide transfer.[28] Remarkably, Cys104 was not a ligand in the structures of both mouse Zn-ISCU and human NFS1-ISD11-ACP-Zn-ISCU complexes, but remained very close to the zinc ion at 3.9 Å and 3.6 Å, respectively, which might be necessary for persulfide transfer. Finally, binding of FXN to the human NFS1-ISD11-ACP-Zn-ISCU complex (PDB code 6NZU)[29] was shown to modify the coordination sphere of the zinc center by pushing aside Cys35 and His103, while allowing Cys104 to bind to the zinc center, most likely to promote persulfide transfer to Cys104. Altogether, these data point to a structural flexibility of the metal-binding site that is probably required to enable persulfide transfer, persulfide reduction, formation of the [2Fe2S] cluster and its accommodation within the assembly site. The structural flexibility of the metal center is intrinsically linked to the metamorphic nature of ISCU that exists in two interconverting forms in solution, a structured (S) and a disordered (D) state.[12,31,32] The binding of a metal ion (zinc or iron) stabilizes the S state by gathering the ligands of the assembly site that belong to distinct secondary structure elements of the protein.[30-32] The overall flexibility of ISCU is thus a key feature of this protein to facilitate structural remodeling of the assembly site during Fe-S cluster assembly.

However, few data are available regarding the iron-containing form of ISCU (Fe-ISCU).[12,33-35] Analysis by circular dichroism (CD) and Mössbauer spectroscopies showed that the ferrous iron initially binds to a cysteine-rich site in mouse ISCU.[12] Site-directed mutagenesis identified Cys35, Cys61 and Asp37 as potential ligands, which suggested that iron binds to the assembly site of mouse ISCU. However, this model was challenged by other studies.[33-35] X-ray absorption (XAS) spectroscopy analysis of prokaryotic and eukaryotic ISCU proteins from *Thermotoga maritima*, *Saccharomyces cerevisiae*, *Drosophila melanogaster* and *Homo sapiens* indicated that iron binds to another site containing exclusively nitrogen and oxygen ligands, suggesting the existence of an auxiliary binding site in ISCU. Moreover, the binding of a second iron into *Escherichia coli* IscU, before sulfur acquisition from IscS, the homolog of NFS1, was reported by native mass spectrometry.[36] The authors suggested that a binuclear iron center is initially formed in ISCU. However, no data was provided to show that both iron ions actually bind to the same site. Binding of the second iron was observed at high concentration of iron over ISCU, suggesting adventitious iron association rather than specific binding. These data therefore raise important questions about the location, structure and conserved nature of the iron-binding site as well as the mechanism of iron insertion into ISCU.

Here, we have examined the iron-binding properties of prokaryotic and eukaryotic ISCU proteins from the bacteria *Escherichia coli*, the fungus *Chaetomium thermophilum* and mammalians *Mus musculus* and *Homo sapiens*. Using CD and Mössbauer spectroscopies, we found that iron exclusively binds to the cysteine-rich assembly site of both prokaryotic and eukaryotic ISCU proteins. Iron outside of the cysteine-rich assembly site is either free or bound to aggregated ISCU, which

questions the existence of an auxiliary site in ISCU. The analysis of the assembly site properties revealed that iron binding is sensitive to the pH, the nature of the buffer and the oligomeric state of the protein. The structural characterization of the assembly site by site-directed mutagenesis, CD, NMR, XAS, EPR and Mössbauer spectroscopies show that the iron is ligated by either one or two cysteine residues of the assembly site with the cysteine receptor Cys104 at a very close distance and able to directly bind to the iron center. These data provide evidence that the insertion of a ferrous iron in the assembly site of ISCU is a conserved process to initiate Fe-S cluster assembly and the spectroscopic analysis establish a structural basis to elucidate the Fe-S cluster assembly mechanism.

Results and discussion

Monomeric ISCU proteins bind iron in a cysteine-rich site

We first assessed the iron-binding abilities of a series of ISCU proteins from prokaryotic and eukaryotic organisms: *E. coli* (*Ec*), *C. thermophilum* (*Ct*), *M. musculus* (*Mm*) and *H. sapiens* (*Hs*). As previously reported, ISCU proteins expressed in bacteria co-purify with zinc in the assembly site that needs to be removed to enable iron insertion.[12] To remove zinc, the ISCU proteins were incubated with DTPA and then purified by size exclusion chromatography (SEC). The chromatograms showed two prominent peaks, a major one between 65 and 85 mL accounting for about 80% of the ISCU and another at 45 mL associated with a high molecular weight (HMW) species (**Fig. 1a**). The elution volumes of the major species were associated with molecular weights of 16, 12, 22 and 26 kDa for *Ec*, *Ct*, *Mm* and *Hs* ISCU, respectively, consistent with monomeric forms for *Ec* and *Ct* ISCU and between monomeric and dimeric for *Mm* and *Hs* ISCU (**Supplementary Table 1**). When *Mm* apo-ISCU was loaded with zinc to stabilize its structured state, it was eluted at a lower volume corresponding to an apparent molecular weight of 17 kDa, consistent with a monomeric form (**Fig. 1b**, **Supplementary Table 1**). Similar results were obtained for *Hs* ISCU (not shown). The higher elution volumes of both *Mm* and *Hs* ISCU were thus linked to their disordered states that were previously shown to be the predominant forms.[12,37] The HMW species were eluted at the void volume, indicating that their size exceeded the exclusion limit of the column close to 100 kDa (**Supplementary Fig. S1a**). When ISCU was loaded onto a Superdex 200, which has an exclusion limit of approximately 1,500 kDa (**Supplementary Fig. S1b**), HMW species were still eluted at void volume (**Supplementary Fig. S1c**), suggesting that the oligomers would contain more than 100 subunits, pointing to aggregated proteins rather than oligomers. When the fraction of monomeric *Mm* ISCU was injected into the SEC column, the HMW species did not appear immediately but after a longer incubation period of 18 h at 4°C (**Fig. 1b**), which was consistent with an aggregation process rather than an oligomeric equilibrium. Indeed, when the monomer was subjected to concentration/dilution cycles on centrifugal membrane filters, we observed the immediate formation of HMW species that could not re-equilibrate toward the monomer upon dilution (**Fig. 1b**). These are typical features of irreversible aggregation processes, indicating that the HMW species are aggregates.

We then assessed the ability of monomeric ISCU proteins to bind iron in the assembly site using circular dichroism (CD) to detect specific Cys → Fe^{II} ligand to metal charge transfer (LMCT) bands that are expected in the 250 - 350 nm region.[12,38] ISCU proteins contain three strictly conserved cysteine residues (Cys35, Cys61 and Cys104 in mouse numbering) that belong to the assembly site.[12,21] *Ct*, *Mm* and *Hs* ISCU contain an additional cysteine (Cys96) that is not conserved and is dispensable for activity in *Mm* ISCU.[12] All the monomeric apo-ISCU proteins incubated with 1.0 equivalent of ferrous iron displayed the typical LMCT bands indicating that iron was inserted in the assembly site of these proteins (**Fig. 1c**).[12] Previous data showed that a single iron binds to the assembly site in *Mm* ISCU with a CD signal of - 30 mdeg at 275 nm for 80 μM of iron in the assembly site based on NMR quantifications,[12]

yielding an absorption coefficient of - 375 deg.cm^{-1}.M^{-1}. These data also allowed estimation of the K_d of iron in *Mm* ISCU based on the amount of apo-ISCU remaining. In a sample containing 100 µM of apo-ISCU and 100 µM of iron, about 20 % of ISCU was not binding iron, which yielded a K_d of 5 µM. By assuming the same K_d and absorption coefficient for all ISCU proteins, the value of the peak at 275 nm for *Ec*, *Ct*, *Mm* and *Hs* ISCU (- 26, - 28, - 32 and - 35 mdeg) indicated that about 70, 75, 85 and 95 % of the iron was bound to the assembly site upon addition of 1.0 molar equivalent of iron, respectively.

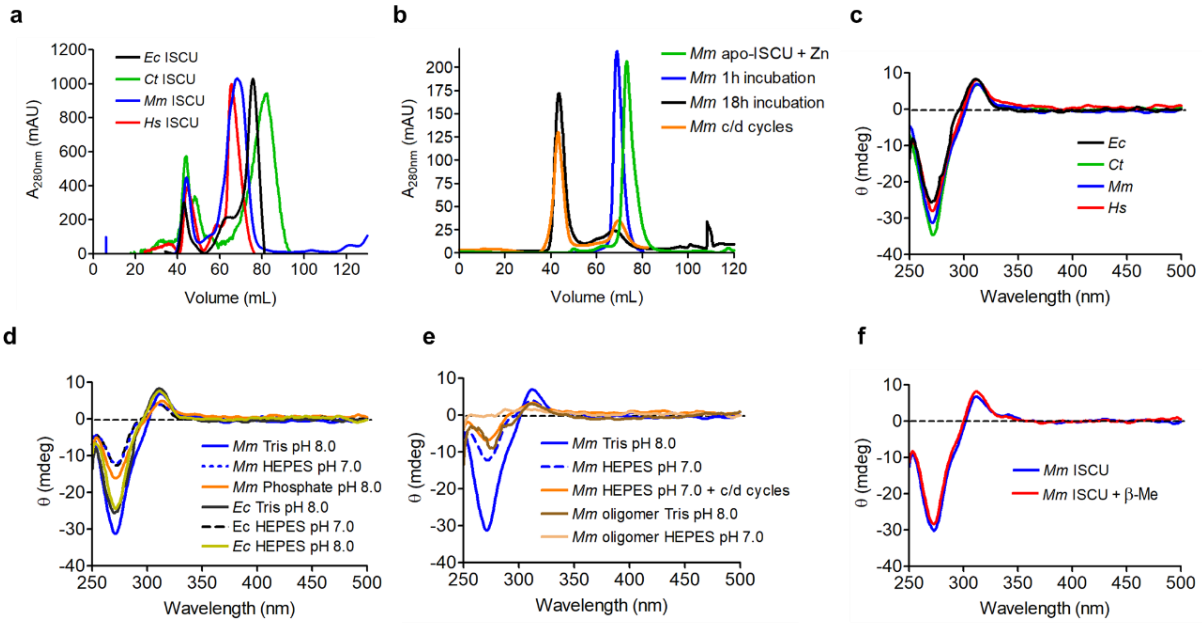

Figure 1: Effect of oligomerization and pH on iron insertion in selected ISCU proteins
(**a**) Size-exclusion chromatograms of *Ec*, *Ct*, *Mm* and *Hs* apo-ISCU proteins. (**b**) Size-exclusion chromatograms of purified monomeric *Mm* apo-ISCU incubated with zinc (apo-ISCU + Zn), incubated for 1 h at 20°C or 18 h at 4°C as indicated and after 5 concentration/dilution cycles (c/d cycles). (**c**) CD spectra of monomeric *Ec*, *Ct*, *Mm* and *Hs* apo-ISCU proteins (100 µM) prepared in Tris pH 8.0 and incubated with 1.0 equivalent of iron. (**d**) CD spectra of monomeric *Mm* and *Ec* apo-ISCU (100 µM) prepared in Tris pH 8.0, HEPES pH 7.0 and phosphate pH 8.0 then incubated with 1.0 equivalent of iron. (**e**) CD spectra of monomeric and oligomeric *Mm* apo-ISCU (100 µM) prepared in Tris pH 8.0, HEPES pH 7.0 and after 5 cycles of concentration/dilution (c/d) in HEPES pH 7.0, incubated with 1.0 equivalent of iron. (**f**) CD spectra of monomeric *Mm* apo-ISCU (100 µM) prepared in Tris pH 8.0 with and without 5 mM of β-mercaptoethanol (β-Me) and incubated with 1.0 equivalent of iron.

These data contrast with XAS studies of *T. maritima*, *S. cerevisiae*, *D. melanogaster* and *H. sapiens* ISCU proteins indicating that iron binds to an auxiliary site lacking cysteine residues.[33-35] In those studies, the apo-ISCU proteins were prepared in HEPES buffer at pH 7.0 with β-mercaptoethanol, stored at 4°C in the anaerobic chamber and submitted to concentration/dilution cycles before the addition of iron, which might have favored the formation of aggregates. Our samples were prepared in Tris buffer at pH 8.0. Monomeric apo-ISCU proteins were deoxygenated by desalting with degassed buffer in the anaerobic chamber, incubated for 1 hour at 10°C and stored in the frozen state in liquid nitrogen with glycerol. Freshly thawed monomeric apo-ISCU proteins were then incubated with iron. We thus tested the effects of the buffer, pH and aggregation on iron insertion. We found that iron binding to the assembly site of ISCU was sensitive to pH, with about 75 % and 65 % decreased iron content

from pH 8.0 to 7.0 in *Mm* and *Ec* ISCU, respectively (**Fig. 1d**). The nature of the buffer also impacted iron binding, with phosphate being much less efficient than HEPES and Tris (**Fig. 1d**). After several concentration/dilution cycles, SEC showed that *Mm* apo-ISCU was mainly aggregated (**Fig. 1b**), which correlated with a 50 % decrease in iron binding to the assembly site at pH 7.0 (**Fig. 1e**). Iron binding to the assembly site of the aggregated form of ISCU collected after SEC was strongly diminished at pH 8.0 and totally abolished at pH 7.0 (**Fig. 1e**). In contrast, we found that the addition of β-mercaptoethanol did not affect the amount of iron bound to the assembly site (**Fig. 1f**). Altogether, these data pointed to critical influences of the pH, the nature of the buffer and the aggregation state of ISCU on the amount of iron bound to the assembly site of ISCU, suggesting that the iron that did not bind to the assembly site was bound to the auxiliary site.

To characterize the presence of a putative auxiliary site in ISCU, the *Hs*, *Mm* and *Ec* proteins were analyzed by Mössbauer spectroscopy (**Supplementary Fig. S2**, **Supplementary Tables 2a, 2b and 2c**). Monomeric *Hs* apo-ISCU was prepared in conditions that would promote the binding of iron to the auxiliary site: different buffers (Tris, HEPES and phosphate) and pH (7.0 and 8.0) and after concentration/dilution cycles in HEPES pH 7.0 (**Supplementary Fig. S2**, HEPES c/d). The *Hs* apo proteins were prepared at concentrations of 1 to 2 mM then incubated with one molar equivalent of ferrous iron. A sample of *Mm* apo-ISCU prepared in Tris pH 8.0 was incubated with two equivalents of ferrous iron to allow filling of both the assembly and auxiliary sites (**Supplementary Fig. S2**, Tris + 2 Fe). Samples of free iron were prepared in the same conditions to discriminate the signals of free iron from ISCU-bound iron. We also analyzed *Ec* ISCU in Tris pH 8.0 to determine whether iron binding to an auxiliary site was a conserved process (**Supplementary Fig. S2**, **Supplementary Tables 2c**).

The analysis by Mössbauer spectroscopy revealed the presence of two main species attributed to ISCU-bound iron, observed in different proportions depending on biochemical conditions (**Fig. 2a**). The remaining iron was distributed between three species with parameters identical to those of free iron (**Fig. 2a**). A minor species with an isomer shift of 0.45 mms^{-1} was attributed to free ferric iron. The main ISCU-bound species was characterized by an isomer shift of 0.87 - 0.89 mms^{-1}, identical to the value reported for iron bound to the assembly site of *Mm* ISCU,[12] in which the iron was proposed to be coordinated by two cysteine residues as confirmed by the XAS data herein (see XAS section, hereafter referred to as the **2-Cys species**). The second species has an isomer shift in the range of 0.98 to 1.03 mms^{-1} that is in the high range for coordination by two cysteines and too low for an environment lacking cysteine, but matches well to values of Fe^{II} centers coordinated by one cysteine residue.[12,39-44] To further assess the number of cysteine, we analyzed the intensities of the LMCT bands at 330 nm by electronic absorption that is correlated with the number of cysteines. The 2-Cys species and both ferric and ferrous iron also contribute to the absorption at 330 nm and with different intensities depending on the buffer and the pH for the latter (**Supplementary Fig. S3a-f**), we thus determined their respective absorption coefficients. For free irons were determined absorption coefficients from electronic absorption spectra

of ferric and ferrous iron solutions prepared in the selected buffers and pHs (**Supplementary Fig. S3c-f**). An absorption coefficient of 1530 $M^{-1}.cm^{-1}$ was determined for the 2-Cys species based on the spectrum of the Tris pH 8.0 sample (**Supplementary Fig. S3a**), in which the species with δ = 0.98 - 1.03 mms^{-1} is absent. This value was used to calculate the absorption coefficient of the δ = 0.98 - 1.03 mms^{-1} species by considering a coordination by either 1 or 2 cysteines and a value of 765 $M^{-1}.cm^{-1}$ per cysteine residue in all buffers and pHs. We calculated the total absorbance at 330 nm (**Fig. 2b**, light blue and turquoise bars) based on the absorption coefficients of these four species and their relative proportions determined by Mössbauer spectroscopy (**Supplementary Tables S2a** and **S2b**). The comparison of the experimental and calculated absorbance values showed a better agreement for a coordination by one rather than two cysteines (**Fig. 2b**), consistent with the Mössbauer data. We thus attributed the δ = 0.98 - 1.03 mms^{-1} species to a Fe^{II} center coordinated by one cysteine residue (hereafter referred to as the **1-Cys species**). To determine whether the cysteine residue could be the surface exposed non-conserved Cys96 residue, we analyzed a C96S ISCU mutant (**Supplementary Fig. S2**, **Supplementary Tables 2b**, Tris C96S). The Mössbauer data revealed that the 1-Cys species was still present in the C96S mutant and in a similar proportion to the WT, indicating that the iron was not coordinated by Cys96 but by one of the cysteines of the assembly site. The isomer shift of the 1-Cys species was sensitive to the nature of the buffer, suggesting that a buffer molecule might be one of the ligands. The line width of the signal was also larger than for the 2-Cys species, with values in the range of 0.4 to 0.58 mms^{-1} and 0.25 to 0.32 mms^{-1}, respectively, indicating that the 1-Cys species was less structurally defined than the 2-Cys one. Comparison of the CD signal intensity at 275 nm with the proportions of the 2-Cys and 1-Cys species determined by Mössbauer spectroscopy showed that the 1-Cys species did not significantly contribute to the CD signal (**Supplementary Fig. S3g-h**, **Fig. 2c**), which is a characteristic feature of poorly structured molecules. Altogether, these data indicated that the 1-Cys species corresponds to iron bound to a distorted assembly site missing one of the two cysteines, possibly replaced by a buffer molecule.

The quantification by Mössbauer showed that the proportion of the 2-Cys and 1-Cys species varied depending on the buffer, the pH and the aggregation state of ISCU (**Fig. 2a**). In Tris at pH 8.0, only the 2-Cys species was present, accounting for 85 % of total iron, as reported for *Mm* ISCU.[12] The value of 85 % of iron bound to ISCU is close to the expected value of 93 % by considering a Kd of 5 μM. The difference is possibly due to the presence of a slight amount of aggregated ISCU that could not bind iron. When two equivalents of iron were added to *Mm* apo-ISCU prepared in Tris pH 8.0 (**Fig. 2a**, Tris + 2 Fe), free iron increased. Still, no other ISCU-bound species were detected, indicating the absence of any other iron-binding site under these conditions. In HEPES and phosphate buffers, both the 2-Cys and 1-Cys species were present, accounting for about 76 % and 55 % of total iron, respectively, but no other site was detected. At pH 7.0, the amount of iron in the 2-Cys site decreased while the amount of the 1-Cys species increased as well as free iron to such a point that the latter became the major species in phosphate buffer (96 %).

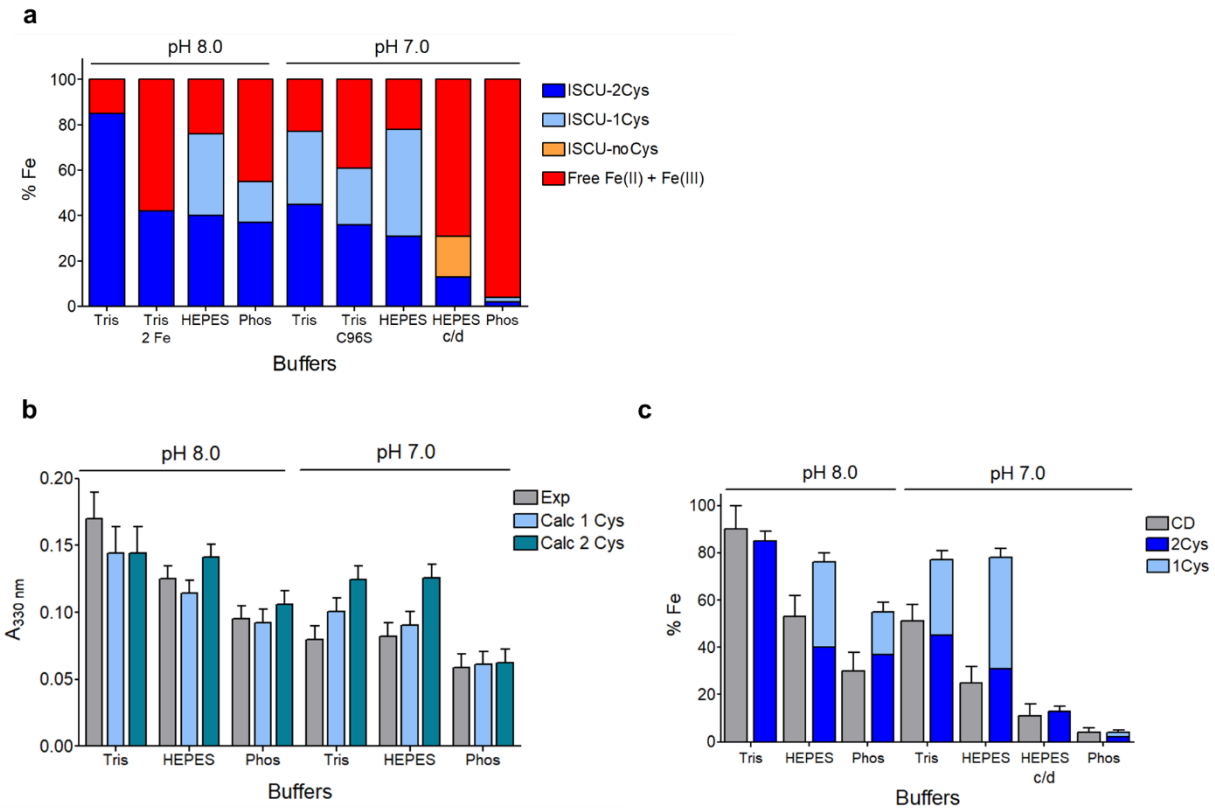

Figure 2: Characterization of the iron-binding sites in *Hs* and *Mm* ISCU by Mössbauer spectroscopy (**a**) Plot of the percentage of iron present as ISCU-bound species (2-Cys, 1-Cys and no-Cys) and free iron (sum of Fe(II) and Fe(III)) determined by Mössbauer spectroscopy from samples of WT *Hs* apo-ISCU (**Supplementary Tables 2a and 2b**) prepared in Tris, HEPES and phosphate at pH 8.0 and 7.0 and from a sample prepared in HEPES at pH 7.0 after 5 concentration/dilution cycles (**HEPES c/d**). C96S *Hs* apo-ISCU was prepared in Tris pH 7.0 (**Tris C96S**). The apo-proteins were then incubated with 1.0 equivalent of iron. *Mm* apo-ISCU was prepared in Tris pH 8.0 and incubated with 2.0 equivalents of iron (**Tris + 2 Fe**). (**b**) Plot of experimental absorbance at 330 nm of WT *Hs* apo-ISCU incubated with one equivalent of ferrous iron in selected buffers as indicated (**Exp,** grey bars) and calculated absorbance at 330 nm for a coordination by one (**Calc 1 Cys**, light blue bars) and two (**Calc 2 Cys**, turquoise bars) cysteines for the ISCU-bound iron species with isomer shift of 0.98 to 1.03 mms^{-1} (1-Cys species). WT *Hs* apo-ISCU was prepared at 100 µM and incubated with one equivalent of iron. Absorbance at 330 nm were calculated based on the amounts of the 2-Cys, 1-Cys, ferrous and ferric iron species determined by Mössbauer (**Supplementary Tables 2a and 2b**) and their absorption coefficients determined from their electronic absorption spectra (**supplementary Fig. S3a-f**) in the different buffers and pH, by considering a coordination by one and two cysteines for the 1-Cys species. (**c**) Plot of the percentage of iron in the cysteinyl site determined by CD at 275 nm (grey bars, **supplementary Fig. S3g-h**) compared to the amounts of the 1-Cys (light blue bar) and 2-Cys species (dark blue bar) measured by Mössbauer and normalized to 100 %.

A minor ISCU-bound iron species was detected, characterized by an isomer shift of 1.16 mms^{-1} (**Fig. 2**, HEPES c/d), consistent with a site lacking sulfur with only N/O ligands (hereafter referred to as the **no-Cys species**) that might be assigned to the auxiliary site. However, this species represented a minor proportion of iron (18 %) and was detected only after the *Hs* apo-ISCU protein prepared in HEPES at pH 7.0 was subjected to concentration/dilution cycles, converting most of the monomeric form into aggregates (**Fig. 1b**). In this sample, the amounts of both the 2-Cys and 1-Cys species were drastically decreased, consistent with CD data, while free iron built up (about 65 % of total iron) and the no-Cys species appeared. These data indicated that the no-Cys site was associated with the

aggregation of the protein and thus could not be assigned to a structured monomeric form. This species was previously assigned to non-specifically bound iron in *Mm* ISCU associated with irreversibly disordered ISCU.[12] Altogether, these data indicate that iron binds to the assembly site of ISCU, either in the 2-Cys or 1-Cys form, and that the protein is devoid of any structurally defined auxiliary site with exclusively N/O ligation. Moreover, analysis of iron binding to *Ec* ISCU in Tris pH 8.0 by Mössbauer spectroscopy revealed that the 2-Cys species was the major species accounting for about 65 % of iron, as observed for *Hs* and *Mm* ISCU (**Supplementary Fig. S2 and Table 2c**). The remaining iron was distributed between a minor no-Cys species (12 %) and free iron (26 %). The Mössbauer parameters of the 2-Cys site in *Ec*, *Mm* and *Hs* ISCU were almost the same, indicating nearly identical assembly site structures in these ISCU proteins.

Monomeric ISCU proteins binding iron in the cysteine-rich site are functional

We next examined whether the insertion of iron in the assembly site was correlated with Fe-S cluster assembly activity. Since the amount of the 2-Cys form decreased from pH 8.0 to 7.0 in Tris buffer, we tested Fe-S cluster assembly efficiencies within this pH range. We first assessed the ability of the iron-loaded forms of *Ec*, *Ct*, *Mm* and *Hs* ISCU proteins to assemble Fe-S cluster at pH 8.0 in Tris buffer by reconstituting their corresponding ISC machineries, which include the NFS1-ISD11-ACP complex, FDX2, FDXR and frataxin (FXN) for *Ct*, *Mm* and *Hs* ISCU and IscS, Fdx and FdxR for the *Ec* IscU. Since Fe-S clusters can also be assembled via a non-physiological route in the absence of the reductase systems (FDX2-FDXR and Fdx-FdxR), we also monitored the rates of Fe-S cluster assembly in the absence of these systems to assess the physiological relevance of these reconstitutions.[12] In the presence of the complete ISC machineries, all the ISCU proteins supported Fe-S cluster assembly (**Fig. 3a, +Fdx**) and at comparable rates, while the reactions were strongly impaired in the absence of the FDX2-FDXR / Fdx-FdxR reductase system (**Fig. 3a, -Fdx**). This indicated that the Fe-S cluster reconstitutions with the whole ISC machineries were physiologically relevant.

We next investigated the effect of pH on two ISC machineries, *Hs* and *Ec* ISC, as representatives of eukaryotic and prokaryotic organisms. As the pH decreased from 8.0 to 7.2, both the *Hs* (**Fig. 3b**) and *Ec* (**Fig. 3c**) ISC machineries were less efficient. Two main features of the kinetics were affected: the yield in [2Fe2S] clusters, estimated by measuring the value of the plateau at the end of the reaction, and the initial rate of Fe-S cluster synthesis. The yields in [2Fe2S] clusters were decreased by about 20 % for both machineries after 30 minutes of reaction from pH 8.0 to 7.2 (**Fig. 3d**). This decrease was lower than the ~ 60 - 65 % initial loss of iron inserted in the assembly site from pH 8.0 to 7.2 in *Hs* (**Fig. 3f**) and *Ec* (**Fig. 3g**) ISCU, since equilibrium between free and ISCU-bound iron most likely allows iron insertion as the reaction proceeds. A more prominent effect of pH was observed on the rate of assembly with decreases of about 70 % for both the *Hs* and *Ec* ISC machineries, from pH 8.0 to 7.2 (**Fig. 3e**), correlated with a similar decrease in the amount of iron into the assembly site (**Fig. 3f, 3g**). Although other steps of the Fe-S cluster assembly reaction might be sensitive to pH, such as persulfide transfer

and reduction (**scheme 1**, steps 4 and 5), the similar effects of pH on iron content and Fe-S cluster assembly suggest that iron insertion at the assembly site is correlated with a more efficient assembly reaction.

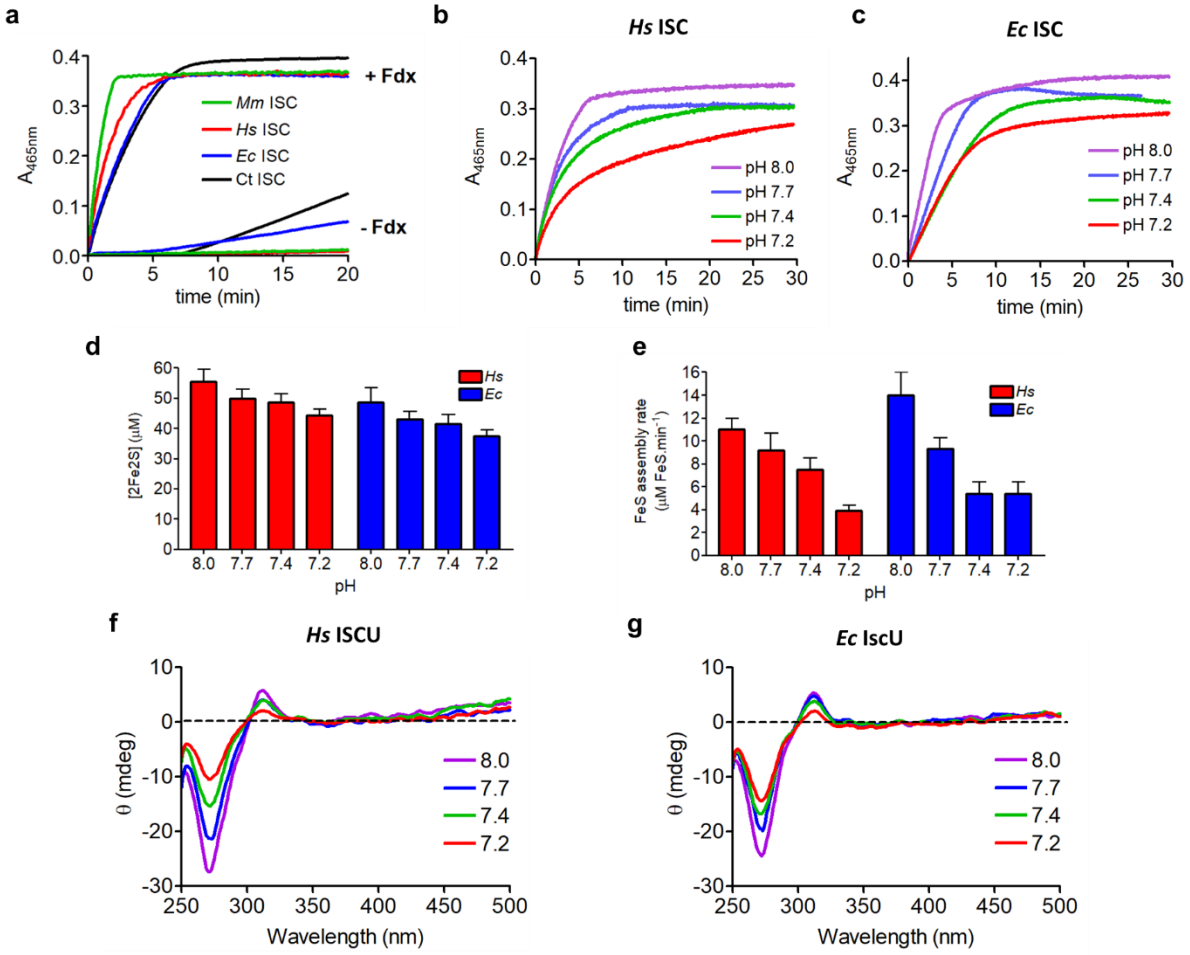

Figure 3: Effect of pH on Fe-S cluster assembly by selected ISC machineries
(**a**) Fe-S cluster assembly assays of monomeric *Ec*, *Ct*, *Mm*, *Hs* ISCU in Tris pH 8.0 with their corresponding ISC machineries in reactions containing (+ Fdx) and lacking (- Fdx) Fdx and FdxR. The mouse ISC machinery was used for *Ct* ISCU. (**b, c**) Fe-S cluster assembly assays of the *Hs* (**b**) and *Ec* (**c**) ISC machineries in Tris at different pH (8.0, 7.7, 7.4, 7.2). (**d**, **e**) Plot of the final yield in [2Fe2S] clusters (**d**) and rate of Fe-S cluster assembly (**d**) at different pH of the reactions presented in b and c. (**f**, **g**) CD spectra of monomeric *Hs* (**f**) and *Ec* (**g**) apo-ISCU prepared in Tris buffer at pH 8.0, 7.7, 7.4 and 7.2 and incubated with 1.0 equivalent of iron.

So far, our data pointed out that the 2-Cys species was the functional form for Fe-S cluster biosynthesis. To provide a complete structural characterization of this species by NMR, XAS and EPR spectroscopies, we prepared *Mm* ISCU in Tris buffer pH 8.0 as these conditions yielded the highest proportion of the 2-Cys species. Furthermore, to prevent the contribution from free iron that would preclude interpretations of the XAS and EPR spectra, the *Mm* apo-ISCU protein was incubated with sub-stoichiometric amounts of iron for these studies, which ensures that iron was exclusively in the 2-Cys form (referred to **Fe-ISCU**) as previously showed by Mössbauer spectroscopy.[12]

Paramagnetic NMR shows that iron binds to the assembly site of *Mm* ISCU

We first analyzed *Mm* Fe-ISCU by NMR to localize the iron-binding site within the structure of ISCU by mapping the perturbations induced by the Fe^{II} center on the 2D ^{1}H-^{15}N HSQC spectrum of ISCU. The paramagnetic state of the Fe^{II} center (S = 2) results in signal broadening in the proximity of the paramagnetic center, due to paramagnetic relaxation enhancement (PRE).[45] For more distant atoms, PRE decreases and signals can be observed. Compared to a diamagnetic reference, these signals display chemical shift perturbations corresponding to pseudo-contact shifts (PCSs). PCSs are sensitive to the distance to the paramagnetic center and to the orientation with respect to the paramagnetic susceptibility tensor.[46] To assess PCS perturbations in Fe-ISCU we used zinc loaded ISCU (Zn-ISCU) as a diamagnetic reference.

The ^{1}H-^{15}N HSQC spectrum of Zn-ISCU was assigned (104 out of 129 amide signals) using standard three-dimensional NMR experiments (**Fig. 4a**, red contours). We then analyzed apo-ISCU at a concentration of 100 μM incubated with one molar equivalent of Fe^{2+} (**Fig. 4a**, blue contours). ISCU is a metamorphic protein that exists in solution in two states, a structured (S) and a disordered (D) one, that are in equilibrium.[31,32] The binding of iron in the assembly site stabilized the S state as demonstrated by the overall signal dispersion, equivalent to that induced by zinc binding (**Fig. 4a**).[12] The broad signal in the center of the spectrum showed that about ~20 % of ISCU was still in the D state. Several signals disappeared due to PRE that were attributed to residues binding the iron ion or very close to it. ISCU residues with large line broadening included the strictly conserved residues binding zinc in the assembly site and the residues next to them (Ala32-Val38, Thr58-Ala71, Lys101-Asp110) (**Fig. 4b)**. Other weak signals were shifted with respect to Zn-ISCU due to PCSs. For many residues, PCSs were nearly the same within amide pairs, and chemical shift perturbations of the ^{1}H and ^{15}N nuclei could be visualized as diagonal lines in the ^{1}H-^{15}N HSQC spectrum (**Fig. 4a**), facilitating assignment transfer: 77 out of 129 amide signals were assigned for iron-loaded ISCU by this means. Residues displaying PCSs and attenuated PRE were in the vicinity of the zinc ligands, but more distant from the paramagnetic center. We mapped Fe^{2+} binding by plotting PREs and PCSs on the structure of *Mm* Zn-ISCU (**Fig. 4c**)**.** The PCS $\Delta\chi$ tensor was fitted with the FANTEN software accessible through the WeNMR portal,[47] without using the coordinates of the Zn atom as an *a priori* information of the position of the paramagnetic metal center. The $\Delta\chi$ tensor was fitted using 118 ^{1}H and ^{15}N PCS, yielding a Q-factor of 0.245, and is represented with PCS iso-surfaces on the structure of Zn-ISCU (**Fig. 4d**). Calculated and observed PCSs correlated rather well (**Fig. 4d**). Taken together, these results indicate that Fe^{2+} binds to ISCU by occupying the Zn-binding site in the structured state of ISCU.

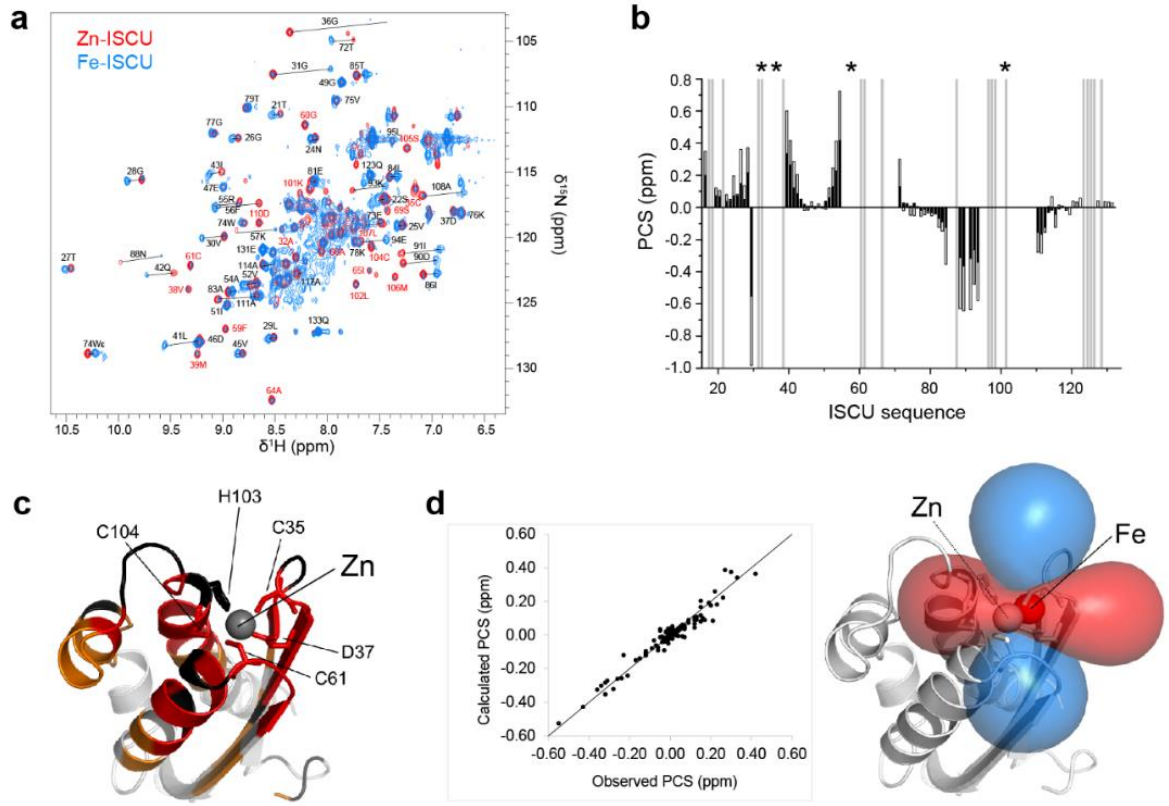

Figure 4: Mapping of the Fe^{2+} binding site in *Mm* Fe-ISCU by paramagnetic NMR
(**a**) Superimposed ^{1}H-^{15}N HSQC spectra of apo-ISCU (1 mM) loaded with 1.0 equivalent of zinc (Zn-ISCU, red contours) or iron (Fe-ISCU, blue contours). Amide assignments are indicated for notable signals. Zn-ISCU signals for which the Fe-ISCU is broadened out by PRE are labelled in red. Notable PCSs are indicated by diagonal lines connecting Zn-ISCU and Fe-ISCU signals. (**b**) PCSs are plotted as stacked bar graphs for observable signals in Fe-ISCU versus Zn-ISCU in both ^{1}H (black) and ^{15}N (white) dimensions. Grey zones correspond to unassigned or proline residues in the Zn-ISCU form. The position of Zn-coordinating residues (black stars) is indicated on top. (**c**) Mapping of Fe^{2+}-induced PREs and/or PCSs onto the structure of *Mm* Zn-ISCU (PDB code 1WFZ, in cartoon). Residues with either strong PRE (complete signal broadening) or ^{1}H and ^{15}N PCS values < -0.1 ppm or > 0.2 ppm are colored in red and orange, respectively. Residues that could not be assigned in Zn-ISCU are colored in black. Zn is represented as a gray sphere and the five invariant residues of the assembly site (Cys35, Asp37, Cys61, His103 and Cys104) are shown in sticks. (**d**) The $\Delta\chi$ tensor was fitted using ^{1}H and ^{15}N PCSs. The correlation between calculated and observed PCS is plotted (left panel). PCS isosurfaces (+1 ppm in blue and -1 ppm in red) were superimposed on the structure of *Mm* Zn-ISCU (right panel). The fitted axial and rhombic values are $\Delta\chi_{ax} = 4.26 \pm 0.12\ 10^{-32}\ m^3$ and $\Delta\chi_{rh} = -1.74 \pm 0.17\ 10^{-32}\ m^3$. The Fe center is represented by a red sphere next to the Zn position (pale red sphere).

Characterization of the iron-binding site of *Mm* ISCU by XAS spectroscopy

We next implemented Fe K-edge X-ray absorption spectroscopy to investigate the structure of the iron center of *Mm* Fe-ISCU. Apo-ISCU was prepared at a concentration of 3 mM in Tris pH 8.0 and was incubated with 0.7 equivalent of iron, which is expected to yield 99 % of iron-loaded ISCU by considering a K_d value of 5 μM. We first analyzed the EXAFS domain of the XAS spectrum (**Fig. 5a, 5b and Table 1**). By setting all parameters free, the fits yielded an average number of four coordinating atoms: two nitrogen/oxygen and two sulfurs (**Table 1, fit #1**). Since the assembly site of ISCU encompasses three cysteines, one aspartate and one histidine, we also performed a series of fits in which the number and the nature of backscattering atoms were constrained to test combinations of three, four and five sulfurs (S) and nitrogen/oxygen (N/O) donating atoms (**Table 1, fits #2 to #9**). We also included fits with exclusively N/O atoms to test the possibility that iron binds to the alternative site. The best fit (**fit #5)** was obtained with four coordinating atoms, two N/O centered at 2.05 Å and two S centered at 2.34 Å. The nature, number and distances of the coordinating atoms were identical to those obtained with the fit performed by leaving all the parameters floating (**fit #1**). This strengthens the EXAFS analysis with only four coordinating atoms, two N/O and two S.

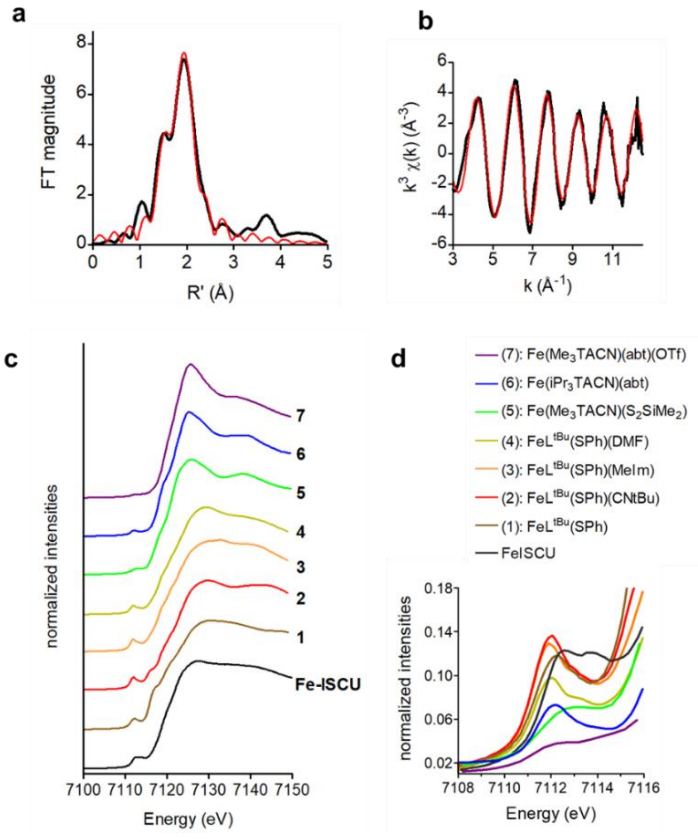

Figure 5: XAS spectra at the Fe-K edge of Fe-ISCU and model compounds.
(**a**, **b**) Fourier transform (a) and unfiltered EXAFS spectrum (b) of *Mm* apo-ISCU (3 mM) in Tris buffer pH 8.0 incubated with 2.1 mM of iron (over a k range of 3 to 13 $Å^{-1}$). Experimental data, black lines; simulation data, red lines. Fit parameters are reported in Table 1 (Fit #1). (**c**, **d**) Normalized XANES spectra (c) and expansion of the pre-edge region (d) for Fe-ISCU and the model compounds $Fe^{II}L^{tBu}$(SPh) (**1**) $Fe^{II}L^{tBu}$(SPh)(CNtBu) (**2**), $Fe^{II}L^{tBu}$(SPh)(MeIm) (**3**), $Fe^{II}L^{tBu}$(SPh)(DMF) (**4**), $Fe^{II}(Me_3TACN)(S_2SiMe_2)$ (**5**), $Fe^{II}(iPr_3TACN)$(abt) (**6**), $Fe^{II}(Me_3TACN)$(abt)(OTf) (**7**) (see **Supplementary Fig. S4** for structures).

Table 1: Parameters from EXAFS fits of Fe-ISCU

CN, total number of backscattering atoms, [a] shell containing absorber: Fe (iron) and backscattering atoms: N (nitrogen), O (oxygen), S (sulfur). [b] number of backscattering atoms set as a free parameter for fit #1 (the standard deviation of the last digit is indicated in brackets) and fixed for fits #2 to #9. [c] average Debye–Waller factor x 10^3 ± 0.1. [d] average Fe-backscatter distance ± 0.04 Å. [e] R-factor indicating goodness of fit (see methods for EXAFS fits).

Fit #	*CN*	*Shell* [a]	*N* [b]	*σ^2 (Å^2)* [c]	*R (Å)* [d]	*R-factor* [e]
1	4	Fe-O/N Fe-S	2.0 (5) 2.1 (5)	4.1 2.4	2.05 2.34	0.020
2	3	Fe-O/N Fe-S	2 1	1.5 0.9	2.09 2.35	0.150
3	4	Fe-O/N Fe-S	3 1	4.2 2.4	2.10 2.35	0.190
4	4	Fe-O/N Fe-S	1 3	9.1 5.2	2.04 2.33	0.049
5	4	Fe-O/N Fe-S	2 2	4.1 2.4	2.05 2.34	0.019
6	5	Fe-O/N Fe-S	3 2	5.8 3.2	2.07 2.34	0.050
7	5	Fe-O/N Fe-S	2 3	9.1 5.2	2.04 2.33	0.043
8	6	Fe-O/N Fe-O/N	1 5	1.1 3.4	2.01 2.19	0.250
9	6	Fe-O/N Fe-O/N	2 4	2.0 1.7	2.01 2.19	0.220

We next analyzed the XANES spectrum of Fe-ISCU and a series of structurally characterized Fe^{II} model compounds, with coordination spheres including sulfurs to provide the most relevant comparisons with Fe-ISCU (**Fig. 5c, 5d, Table 2, supplementary Fig. S4, S5**). The XANES spectrum of Fe-ISCU displayed two pre-edge peaks at 7112.3 eV and 7113.7 eV attributed to 1s→3d transitions and shoulders on the rising edge between 7115 – 7125 eV attributed to 1s→4p transitions (**Fig. 5c, 5d, Table 2**). Strikingly, the overall shape of the XANES spectra of Fe-ISCU exhibited strong similarities with 3- and 4-coordinated tetrahedral complexes, with a smooth maximum between 7125 – 7130 eV, while 5- and 6-coordinated complexes were characterized by a more prominent maximum in this region. This suggested that the Fe^{II} center of Fe-ISCU is 3- or 4-coordinated. The intensity and the energy of the pre-edge transitions are usually good indicators of the number of ligands, the geometry and the nature of the coordinating atoms. The dipole allowed 1s→3d transitions gain intensity through hybridization of the 3d (t_{2g}) orbitals with the overlying 4p orbitals, which relies on the non-centrosymmetric character of the ligand field.[48-51] Thereby, tetrahedral complexes display more intense pre-edge features than trigonal pyramid, square planar and octahedral ones.[48-51] The value of the integrated area under the pre-edge peaks of Fe-ISCU was much higher than 5- and 6-coordinated complexes as well as 4-coordinated square planar centers but fell into the range of 4-coordinated tetrahedral Fe^{II} complexes (**Table 2**). The energy of the 1s→3d transitions is also sensitive to the covalency of the metal-ligand bond. As sulfurs establish more covalent bonds than nitrogen and oxygen, one would expect that the energy increases with the number of sulfurs. Indeed, the plot of the energy of the first pre-edge peak against the number

of sulfurs provided a relatively good correlation in the series of 4-coordinated tetrahedral Fe^{II} complexes (**Supplementary Fig. S6**). Thereby, the value for Fe-ISCU was indicative of the presence of two or three sulfurs coordinating the Fe^{II} center, which was consistent with the EXAFS data.

In conclusion, the analysis of the XANES spectrum corroborated and complemented the EXAFS analysis, which together indicated that the Fe^{II} center in Fe-ISCU is 4-coordinated in a distorted tetrahedral geometry by two sulfurs and two nitrogen/oxygen ligands. This set of ligands is consistent with a coordination by two cysteines and two aspartate or histidine residues, as earlier proposed based on site-directed mutagenesis.[12]

Table 2: Pre-edge parameters for Fe-ISCU and selected 3-, 4-, 5- and 6-coordinated Fe^{II} model compounds. [a] C.A., coordinating atoms. [b] standard deviation of ± 3.5 %. See Methods and **Supplementary Fig. S5** for fits of XANES data for Fe-ISCU and complexes (5-7).

Sample	Geometry	C.A.[a]	Pre-edge peaks 1s → 3d (eV)	Pre-edge area x 10^2 ($Å^2$)	Ref
FeISCU		2S, 2N/O	7112.3 ; 7113.7	25.2 [b]	This work
	3-coordinated complexes				
FeL^{tBu}(SPh) (**1**)	D3h	1S, 2N	7112.2	23.4	[48]
	4-coordinated complexes				
Rubredoxin AlkG	Td	4S	7112.8	17.5	[52]
$[Fe(SPh)_4]^{2-}$	Td	4S	7112.5	30	[53]
$[Fe_2(bis(benzimidazolato)_2S_2]^{4-}$	Td	2S, 2N	7112.1	25	[51,54]
FeL^{tBu}(SPh)(CNtBu) (**2**)	Td	1S, 1C, 2N	7111.9 ; 7113.4	28.3	[48]
FeL^{tBu}(SPh)(MeIm) (**3**)	Td	1S, 3N	7111.9 ; 7113.2	23.5	[48]
$Fe(HB(3,5\text{-}^{i}Pr_2pz)_3(SC_6H_4\text{-}p\text{-}NO_2)$	Td	1S, 3N	7111.5	21	[49]
FeL^{tBu}(SPh)(DMF) (**4**)	Td	1S, 2N, 1O	7111.9 ; 7113.4	18.9	[48]
$Fe(HB(3,5\text{-}^{i}Pr_2pz)_3(OC_6H_4\text{-}p\text{-}Cl)$	Td	3N, 1O	7111.5	18.5	[49]
Gillespite ($BaFeSi_4O_{10}$)	D4h	4O	7111.7 ; 7113.2	5.3	[50]
$Fe(HB(3,5\text{-}iPr_2pz)_3)Cl$	Td	3N, 1Cl	7111.6 ; 7113.2	20	[50]
$[FeCl_4]^{2-}$	Td	4Cl	7111.6 ; 7113.1	13	[50]
	5-coordinated complexes				
$Fe(Me_3TACN)(S_2SiMe_2)$ (**5**)	C4v	2S, 3N	7112.6 ; 7113.8	10.3 [b]	This work,[55,56]
$[Fe(TMCS)]^{+}$	C4v	1S, 4N	7112.5 ; 7114.4	13.6	[57]
$[Fe(iPr_3TACN)(abt)]^{+}$ (**6**)	C4v	1S, 4N	7112.1 ; 7113.7	12.1 [b]	This work,[58]
$[Fe(TPA)(S\text{-}2,4,6\text{-}Me_3C_6H_2)]^{+}$	C3v	1S, 4N	7112	8.9	[49,59]
$[Fe(TMCSO_2)]^{+}$	C4v	4N, 1O	7112.6	13.4	[57]
$Fe(HB(3,5\text{-}^{i}Pr_2pz)_3(OBz)$	C3v	3N, 2O	7112	10.7	[49]
$[Fe_2(OBz)(et\text{-}HPTB)]^{2+}$	D3h	3N, 2O	7111.7 ; 7113.4	13	[50]
	6-coordinated complexes				
$Fe(Me_3TACN)(abt)(OTf)$ (**7**)	Oh	1S, 4N, 1O	7112.1 ; 7114	6.4 [b]	This work,[58]
IPSN + ACV	Oh	1S, 2N, 3O	7112 ; 7118	12	[60]
IPSN	Oh	2N, 4O	7112	8	[60]
$[Fe_2(salmp)_2]^{2-}$	Oh	2N, 4O	7111.4 ; 7113.6	5	[50]

Identification of the protein ligands of the Fe^{II} center by site-directed mutagenesis combined with Mössbauer, CD and EPR spectroscopies

We previously reported results a site-directed mutagenesis study alongside Mössbauer and circular dichroism spectroscopies to identify the ligands of the iron center in *Mm* ISCU.[12] These analyses suggested that the iron is coordinated by Cys35, Cys61, Asp37 and His103, while Cys104 is unbound. These data are consistent with the set of 2S and 2N/O donating atoms determined in the present study by XAS spectroscopy. However, while the data clearly showed that the mutants of Cys35, Cys61 and Asp37 totally abolish iron binding to the assembly site, strongly supporting the conclusion that these residues are ligands of the metal center, the conclusions regarding His103 and Cys104 were less robust. The C104S mutation decreased the affinity of ISCU for iron, suggesting that Cys104 might be ligating or close to the Fe^{II} center in the assembly site.[12] Conversely, the Mössbauer parameters were not affected by the mutation, thus suggesting that Cys104 is not a ligand (**Table 3**). The Mössbauer analysis revealed the presence of two different species (**Table 3**, S_1 and S_2). The parameters of the main species (S_1, 63 %) were identical to those of iron in the assembly site of WT ISCU within the margin error. Therefore, the Mössbauer analysis did not support the idea that Cys104 is ligating or even interacting with the iron center. However, we could not definitely conclude due to the presence of the other species (S_2, 37 %) with parameters indicative of a site without cysteine (δ = 1.23 mms^{-1}).[12] Intriguing results were also obtained with the H103A mutant.[12] This mutant displayed CD absorptions attributed to the characteristic Cys → Fe^{II} LMCT transitions. Although the intensities of these absorptions were much weaker than in the WT protein, these data suggested that iron still binds to the assembly site of the mutant, albeit weakly. However, we could not detect any species with sulfur donating atoms by Mössbauer spectroscopy. This prompted us to re-examine the C104S and H103A mutants of *Mm* ISCU.

We first examined the C104S ISCU mutant. As observed with WT ISCU, a significant proportion of the C104S ISCU mutant was eluted as aggregates by SEC, but the monomer was still the major form (**Fig. 6a, orange curve**). Then, to assess the stability of iron in S_1 and S_2 previously characterized by Mössbauer spectroscopy (**Table 3**), monomeric apo-$ISCU^{C104S}$ prepared at a concentration of 1 mM in Tris pH 8.0 was incubated with 0.5 equivalent of iron. Under these conditions, the Mössbauer spectrum of $ISCU^{C104S}$ showed the presence of a single species, characterized by a doublet with parameters identical to those previously reported for S_1 in C104S incubated with 1.0 equivalent of iron that was attributed to iron in the assembly site (**Fig. 6b, Table 3**). This indicates that iron has a higher affinity for the assembly site than for the iron-binding site of S_2. Indeed, the linewidth of S_2 was much larger than S_1, 0.65 mms^{-1} versus 0.35 mms^{-1}, respectively (**Table 3**), which strongly suggested that S_2 corresponds to non-specifically bound or free iron. Both the isomer shift and the quadrupole splitting of WT ISCU and S_1 in the C104S mutant were identical within the experimental error, which points to an overall conservation of the ligands, the geometry and the bond distances of the Fe^{II} center in the C104S mutant. To strengthen these data, we analyzed the C104S mutant by EPR

spectroscopy. Depending on their zero-field splitting (ZFS) parameters, high spin ferrous iron species (S = 2) exhibit EPR spectra at X-band (ν ~ 9 GHz).[61] EPR spectra of integer-spins can be observed with the microwave magnetic field B_1 either perpendicular or parallel to the applied static magnetic field B_0 but are normally best detected using the parallel mode.[62] We first analyzed WT ISCU prepared at 1 mM incubated with 0.7 equivalent of iron, which is expected to yield 99 % of iron-loaded ISCU by considering a K_d of 5 μM. The X-band parallel mode EPR spectrum of WT Fe-ISCU displayed a derivate peak at g = 14.9 (**Fig. 6c**), corresponding to a transition within the non-Kramers doublet "M_S = ± 2" of the S = 2 Fe^{II} center. To our knowledge, it is the first EPR signal reported for a Fe^{2+}-bound ISCU species. This signature was observed in various Fe-ISCU samples (ISCU proteins incubated with 0.5 - 0.8 eq. of ferrous iron), was not present in a control sample with 0.5 mM Fe^{2+} in buffer and was almost identical for *Mm* and *Ec* ISCU proteins incubated with iron (**Supplementary Fig. S7a**). Furthermore, the intensity of the EPR spectrum of WT *Mm* ISCU was decreased by about 3-fold in phosphate compared to Tris buffer, which confirms the CD and Mössbauer data indicating that the buffer influences the stability of iron within ISCU (**Supplementary Fig. S7b**). The EPR signature was slightly shifted at a higher field (g = 13.4) in the C104S mutant (**Fig. 6c**), showing that the electronic structure of the Fe^{II} center is sensitive to the mutation, which suggests that Cys104 is part of the second shell of residues surrounding the Fe^{II} center.

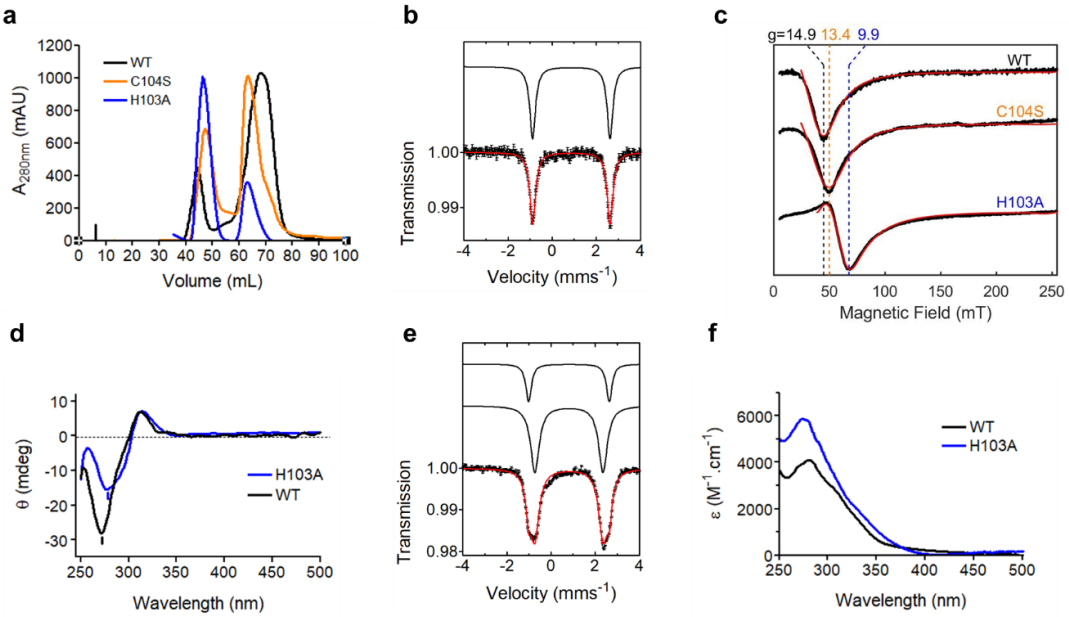

Figure 6: Characterization of the C104S and H103A mutants of *Mm* ISCU
(**a**) SEC analysis of WT, C104S and H103A after removal of the zinc ion. (**b**) Mössbauer spectrum of C104S incubated with 0.5 eq. of ferrous ion. (**c**) Parallel-mode X-band EPR spectra of WT (0.7 mM), C104S (1 mM) and H103A (0.7 mM) ISCU proteins incubated with ferrous iron (0.5 mM) in Tris buffer. EPR recording parameters: temperature, 7 K; microwave frequency, 9.38 GHz; microwave power, 1 mW; modulation amplitude, 0.98 mT. EPR simulations (red lines) were performed assuming an isotropic g = 2 value with a standard deviation parameter of the Gaussian distribution, $\sigma_{E/D}$, of 0.004 (WT), 0.008 (C104S) and 0.016 (H103A). (**d**) CD spectra of WT and H103A incubated with 1 eq. of iron. (**e**) Mössbauer spectrum of H103A incubated with 0.5 eq. of iron. Mössbauer parameters: temperature, 77 K; the solid lines are simulations with parameters given in Table 3; red line, best fit of the experimental data; black lines, components of the simulation. (**f**) Electronic absorption spectra of WT ISCU (100 μM) incubated with 1.0 equivalent of iron (100 μM) and H103A mutant (200 μM) incubated with 0.5 equivalent of iron (100 μM). The absorption of the apo-proteins was subtracted.

Table 3. Mössbauer parameters of WT, C104S and H103A *mM* ISCU

[a] Molar equivalent of ferrous iron added to ISCU. [b] Only parameters for simulation with Set 1 are displayed, parameters for Set 2 are presented in Supplementary Table 3.

Mm ISCU	Eq. Fe[a]	Species	δ (mms^{-1})	ΔE_Q (mms^{-1})	Γ (mms^{-1})	Area (%)	References
WT	0.7	-	0.88 (1)	3.51 (1)	0.35 (1)	100	[12]
C104S	1.0	S_1	0.87 (1)	3.51 (1)	0.35 (1)	63	[12]
		S_2	1.23 (1)	3.15 (1)	0.65 (1)	37	
C104S	0.5	-	0.87 (1)	3.51 (1)	0.35 (1)	100	this work
H103A [b]	0.5	S_1	0.81 (1)	3.08 (1)	0.47 (1)	73 (2)	this work
		S_2	0.81 (1)	3.65 (1)	0.30 (1)	27 (2)	

To assess the effect of the C104S mutation in more detail, we analyzed the zero-field splitting (ZFS) parameters, *E* and *D*, of the Fe^{II} center in the WT ISCU and C104S mutant. We used two different methods: 1) fitting of the temperature dependence data of the EPR signal according to the Boltzmann equation in which the energy states of the $S = 2$ manifold derived from the spin Hamiltonian and 2) numerical simulations (**Supplementary Text 1**). Fittings by the first method were performed assuming an axial zero-field splitting ($E = 0$). The best fits gave *D* parameters of - 6.5 ±1.0 cm^{-1} and - 4.0 ±1.0 cm^{-1} for the Fe^{II} center in WT ISCU and the C104S mutant, respectively (**Supplementary Fig. S8**, **Table 4**). The best fits by numerical simulations were achieved using a Gaussian distribution of the *E*/*D* parameter and yielded *D* and *E*/*D* values of -5.9 cm^{-1} and 0.13 for the WT and -3.5 cm^{-1} and 0.17 for C104S (see legend of **Fig. 6c** and **Table 4** for all simulation parameters). These values were in good agreement with the *D* values estimated from the Boltzmann population distribution.

Table 4. Zero Field Splitting parameters of the $S = 2$ spin state determined by EPR in WT, C104S and H103A *mM* Fe-ISCU

[a] ZFS parameters estimated by two different ways: **Temp.**, from temperature dependence of the low-field EPR signal with Boltzmann population distribution of the "$M_S \pm 2$" sub-level reported in **Fig. S8**. The rhombic ZFS parameter, *E*, could not be determined accurately from the temperature study and therefore fittings were made assuming $E = 0$. **Simul.**, from spectral simulations reported in **Fig. 6c**.

mM ISCU	Method [a]	*D* (cm^{-1})	*E*/*D*	$\lvert E \rvert$ (cm^{-1})
WT	Temp.	- 6.5 (9)	0	0
	Simul.	- 5.9	0.13	0.76
C104S	Temp.	- 4.0 (9)	0	0
	Simul.	- 3.6	0.17	0.6
H103A	Temp.	- 2.5 (9)	0	0
	Simul.	- 0.9	0.31	0.29

Overall, the Mössbauer parameters (δ, ΔE_Q) indicate that the geometry and the ligands of the Fe^{II} center are unchanged between WT and C104S, while the EPR data, which are more sensitive to ZFS parameters, pointed out some variations. The ZFS parameters were shown to be sensitive to small geometrical distortions of the metal center and also to the changes of Lewis basicity of the ligands by remote ligands substituents.[63-65] As the quadrupole splitting is mainly sensitive to variations of the first coordination sphere of the metal, we conclude that the modifications of the ZFS parameters reflect changes from the secondary coordination sphere of the Fe^{II} center in ISCU. In conclusion, Mössbauer and EPR data support the idea that Cys104 is not a ligand but is part of the second shell of residues around the Fe^{II} center, which stabilize the iron in the assembly site.

We next investigated iron binding to the H103A mutant. A retrospective analysis revealed that the cysteine residues were oxidized as disulfide bonds in the samples of the H103A mutant previously analyzed by Mössbauer, which precluded iron insertion in the assembly site (**Supplementary Fig. S9**, lane 2). Furthermore, the SEC analysis indicated a more pronounced susceptibility of the H103A mutant to aggregate than the WT and C104S mutant (**Fig. 6a**). To assess iron binding to H103A, we prepared samples of the H103A mutant under reducing conditions using DTT to keep the cysteines in their reduced states (see **Methods**). Under these conditions, the cysteines of the H103A mutant were fully reduced (**Supplementary Fig. S9**, lane 3). The CD spectra of reduced monomeric H103A incubated with 1.0 equivalent of iron displayed typical CD absorptions attributed to Cys → Fe^{II} LMCT but at slightly lower energies and with reduced intensity for the negative features, compared to WT ISCU (**Fig. 6d**). To assess the possibility that H103A had a lower affinity for iron, we incubated H103A with a higher amount of iron (2.0 equivalents), but the intensity did not increase (**Supplementary Fig. S10a**, ratio 1:2). In contrast, the intensity of the CD signal was increased by approximately 45 % when the concentration of H103A was doubled, keeping iron constant (**Supplementary Fig. S10a**, ratio 2:1). This indicates that about 30% of the H103A ISCU protein could not bind iron in the assembly site with a 1:1 ratio. This might be due to the formation of aggregates during concentration of the monomeric form. Moreover, two distinct peaks were now visible at the 2:1 ratio, at 271 nm and 281 nm, which pointed to the presence of different species depending on the protein:iron ratio.

An EPR signal was still visible in the X-band parallel-mode spectrum of the H103A ISCU mutant but was largely shifted to a higher magnetic field, with a resonance line at g = 9.9 (**Fig. 6c**). From the temperature dependence study of the g = 9.9 signal, we determined an axial parameter, D, of - 2.5 cm^{-1}, a value that may be partly overestimated because the plateau (corresponding to 100% population of the ground state "$M_S \pm 2$" sub-level) could not be reached at the lowest temperature of our experiments (T = 3.6 K, **Supplementary Fig. S8**). The best simulation of the g = 9.9 signal gave parameters of D = - 0.95 cm^{-1} and E/D = 0.31, thus reflecting large changes in the electronic structure of the Fe^{II} center in the H103A mutant. The Mössbauer spectrum of H103A prepared at 2 mM with 0.5 equivalent of iron shows the contribution from two species coordinated by cysteine residues (**Fig. 6e**). Two different sets

of parameters (Set 1 and 2) could fit the experimental data (**Supplementary Table 3**, **Supplementary Text 2**). Set 2 yielded 35 % of a Fe^{II} center coordinated by four sulfurs, which appeared unrealistic in the assembly site that contains only three cysteines. An alternative hypothesis would be that the H103A mutant formed a dimer with a bridging Fe^{II} center, and each subunit provides two cysteines. This was ruled out by SEC analysis showing that iron-loaded H103A was eluted as monomeric Zn-ISCU (**Supplementary Fig. S10b**). Thereby, the hypothesis of set 2 was discarded. Set 1 yielded two species with identical isomer shift but different quadrupole splitting, which pointed to species with the same coordination sphere but slightly different geometries (**Table 3**, S_1 and S_2). Only one signature was detected by EPR, likely because S_1 and S_2 display electronic parameters too close to be resolved at X-band (9 GHz), as shown before for the $Fe[(SPPh_2)_2N]_2$ complex that exhibits two main conformers only distinguishable at high frequencies EPR.[66]

The isomer shift of S_1 and S_2 (δ = 0.81 mms^{-1}) was lower than the value determined for WT ISCU (δ = 0.88 mms^{-1}), which suggested that the number of sulfurs was increased from 2 to 3, and thus that Cys104 replaced His103 since it is the only available cysteine at a close distance to the Fe^{II} center. However, a coordination by two cysteines could not be totally excluded based on the value of the isomer shift.[12] A coordination by two cysteines would be possible if Asp37 switches to the bidentate mode to fill the empty position left by His103. However, the quadrupole splitting was shown to decrease by 1 to 2 mms^{-1} upon switching to the bidentate coordination mode in a series of structurally similar Fe^{II} model complexes,[67] but the quadrupole splitting of S_1 was only decreased by 0.46 mms^{-1} and the value of S_2 was increased. Thus, these changes are not consistent with a switch to the bidentate mode. In contrast, the replacement of His103 by Cys104 could account for small changes in the quadrupole splitting values. To further assess the hypothesis that Cys104 replaces His103, we analyzed the intensities of the LMCT bands that are correlated with the number of cysteines. The intensity of the UV-visible spectra in the LMCT region (200 - 400 nm) was increased in the H103A ISCU mutant compared to the WT protein, which suggested the presence of a higher number of cysteines (**Fig. 6f**). Values in the range of 1800 to 2400 $M^{-1}.cm^{-1}$ were reported for the Fe^{II} center of azurin, which is structurally similar to Fe-ISCU but with a coordination sphere including a single cysteine residue.[40] The value of the absorption coefficients for the most intense peak in Fe-ISCU WT (280 nm) was 4050 $M^{-1}.cm^{-1}$, which fits well with the presence of two cysteines by using an empiric value of ~ 2000 $M^{-1}.cm^{-1}$ per cysteine residue (**Fig. 6f**). The absorption coefficient for the most intense peak in the H103A mutant (275 nm) was approximately 5900 $M^{-1}.cm^{-1}$, consistent with a coordination by three cysteine residues. This value was too high for the set 2 hypothesis from Mössbauer analysis, since 35 % of a Fe^{II} center with four cysteines and 65 % with one cysteine would yield an absorption coefficient between 3500 and 5000 $M^{-1}.cm^{-1}$. These data thus support the hypothesis that in the absence of His103, Cys104 becomes a ligand. The presence of two species with distinct quadrupole splitting values might be explained by different conformations of the $Fe^{II}(Cys)_3(Asp)$ center and could be related to the two similar species detected by CD (**Supplementary**

Fig. S10a). Altogether, these data indicate that H103 is the fourth ligand of the Fe^{II} center in *Mm* Fe-ISCU and suggest that Cys104 can replace it.

Conclusion

Collectively, our data provide an in-depth characterization of the iron insertion process into the ISCU scaffold protein, highlighting the structural flexibility of the Fe-S cluster assembly site and its conserved nature. The SEC analysis showed that *Ec*, *Ct*, *Mm* and *Hs* apo-ISCU are predominantly monomeric proteins, but prone to aggregation in their apo forms. This aggregation process most likely involves the disordered form of apo-ISCU into which hydrophobic regions might be solvent exposed and thus prone to association. CD and Mössbauer analysis showed that monomeric *Ec*, *Ct* and *Hs* ISCU proteins bind iron in a cysteine-rich site as reported for *Mm* ISCU.[12] This iron-binding site was assigned to the Fe-S cluster assembly site that contains three strictly conserved cysteines: Cys35, Cys61 and Cys104 (mouse and human numbering). Mössbauer analysis of *Hs* ISCU further showed that the assembly site exists in two different states with the iron coordinated by either one or two cysteines, referred to as the 1-Cys and 2-Cys species, respectively. The proportion of these two species was strongly dependent on pH and the nature of the buffer. The 2-Cys species was the predominant form at pH 8.0 and its proportion decreased at more acidic pH, from 8.0 to 7.0, while the amount of the 1-Cys species as well as free iron increased. The amount of free iron versus ISCU-bound iron was higher in phosphate than in Tris or HEPES, correlating with the stronger iron-binding affinity of phosphate relative to Tris and HEPES.[68,69] This indicates that iron is in equilibrium between the buffer and ISCU. *In vivo*, where phosphate is one of the main biological buffers, the concentration of free iron may thus override the buffering capacity of phosphate to allow iron acquisition by ISCU. Alternatively, an iron chaperone could promote iron insertion in ISCU, but it would not prevent iron release from ISCU, suggesting instead that the conversion into Fe-S clusters might be the driving force enabling iron use.

To provide in-depth structural analysis of the assembly site, we took advantage of the Tris buffer pH 8.0 conditions in which the 2-Cys species was the only ISCU-bound iron form. Furthermore, to favor ISCU-bound over free iron, apo-ISCU was incubated with sub-stoichiometric amount of iron, which produces samples with iron exclusively in the assembly site. The structural studies of the 2-Cys site in *Mm* ISCU by CD, NMR, XAS, Mössbauer and EPR spectroscopies showed that the Fe^{II} center is coordinated by four strictly conserved residues of the assembly site: Cys35, Asp37, Cys61 and His103 in a close to tetrahedral geometry. The EPR analysis further showed that Cys104, the persulfide acceptor in ISCU, is very close to the iron center, which is probably essential to facilitate persulfide transfer to this residue (**scheme 1**, step 4). The same structural organization was reported for zinc bound to the assembly of ISCU, with Cys35, Asp37, Cys61 and His103 ligating the metal center and Cys104 at a close distance.[1] Since zinc can functionally replace iron for persulfide transfer to Cys104 and the stimulation of this process by FXN,[12] this structural organization is probably critical to enable metal-dependent persulfide transfer and its stimulation by FXN.[13] The CD, EPR and Mössbauer studies also suggest that Cys104 replaces His103 in the H103A mutant by filling the empty position on the iron center. This structural rearrangement is reminiscent of the effect of FXN on the zinc center of the human

NFS1-ISD11-ACP-Zn-ISCU complex that pushes His103 aside and allows Cys104 to replace it.[29] This ability of Cys104 to move toward the iron center by swapping with His103 might thus be a key structural feature enabling iron-dependent persulfide transfer and its acceleration by FXN.

Besides the 2-Cys form, the Mössbauer analysis revealed the existence of another state of the iron in the assembly site, in which it is coordinated by a single cysteine (1-Cys species). The increase of the proportion of the 1-Cys species from pH 8.0 to 7.0 suggests that one of the two cysteines is protonated at pH 7.0 and can no longer bind iron. The Mössbauer analysis further suggests that a buffer molecule replaces the missing cysteine in the 1-Cys species, indicating that the assembly site is solvent exposed. Indeed, the structure of ISCU showed that the assembly site is mostly solvent exposed with only few interactions between the two cysteines ligating the iron and surrounding amino acids.[1] Cys35 appears as the most solvent exposed of the two, without any close contact with other amino acids. Thereby its pKa might be very close to 8.3, the value of free cysteine. The shift from a 2-Cys to a 1-Cys coordination by decreasing pH from 8.0 to 7.0 might thus be explained by protonation of Cys35 that can no longer bind the metal and is replaced by a buffer molecule. Moreover, increase in the 1-Cys form at more acidic pH is correlated with free iron accumulation, suggesting that stabilization of the 1-Cys species impairs iron insertion. The assembly site gathers four amino acids (Cys35, Asp37, Cys61 and His103) belonging to three distinct domains of the protein,[28] the 1-Cys could thus represent an intermediate state of the iron insertion process and stabilizing it would compromise conversion to the 2-Cys state. Interestingly, in the NFS1-Zn-ISCU complex the catalytic cysteine of NFS1 binds to the zinc center by exchange with Cys35,[28] which supports the idea that Cys35 can move within the assembly site. The exchange between the catalytic cysteine of NFS1 and Cys35 is proposed to be the primary step of the iron-dependent persulfide transfer to Cys104 (**scheme 1**, step 4).[13] Therefore, the 1-Cys species might also be a key intermediate of the persulfide transfer process.

The pH studies further showed that the amount of iron in the 2-Cys form was correlated with Fe-S cluster assembly activity, indicating that the 2-Cys form is the functional state. The pH dependency of iron insertion and thereby of the Fe-S cluster biosynthetic activity raises the question of the physiological relevance since pH varies depending on the organism and the cellular compartment hosting the ISC machinery. Iron insertion in the assembly site is more efficient at pH 8.0 for the eukaryotic *Ct*, *Mm* and *Hs* proteins, which is close to the physiological pH of the mitochondrial matrix (~ 8.0) where the ISC machinery is located.[70,71] In bacteria, the internal pH relies on external conditions and thus depends on the environment.[72-75] *E. coli* strains colonize different parts of the gastrointestinal tract, essentially the small intestine, where the pH is acidic, in the range of 6.0 - 7.0, and the colon, where it ranges from 7.0 - 8.5.[74] Thus, the pH dependency of the Fe-S cluster assembly reaction in *E. coli* could be related to adaptation to different physiological conditions and the ability of these bacteria to colonize different parts of the intestinal tract.

Importantly, our results contrast with the XAS studies previously reported for *T. maritima*, *S.cerevisiae*, *D. melanogaster* and *H. sapiens* ISCU proteins which showed that iron was exclusively ligated by N/O ligands, leading to the conclusion that iron initially binds at an auxiliary site containing exclusively N/O ligands before transfer to the assembly site.[33-35] Our data indicate that such a site does not exist in monomeric ISCU proteins from both prokaryotic and eukaryotic organisms (*Ec*, *Ct*, *Mm* and *Hs*) as they bind iron exclusively in the assembly site. Under the conditions used for these XAS studies, HEPES buffer at pH 7.0 and dialysis by concentration/dilution cycles to remove TCEP, we found that apo-ISCU was heavily aggregated due to repeated concentration cycles. Under these conditions, iron was indeed in an N/O environment but as free iron bound to buffer and as an ISCU-bound species without sulfur but associated to aggregated ISCU, together accounting for about 80 – 90 % of total iron. Therefore, sample preparation conditions probably explain findings that iron was bound by N/O ligands.

In summary, our data provide evidence that the direct insertion of iron in the assembly site of ISCU is a conserved process across species, from prokaryotes to eukaryotes, to initiate Fe-S cluster biosynthesis. The spectroscopic characterizations of the assembly site presented here highlight the structural flexibility of this site, which appears critical to allow the rearrangements enabling subsequent persulfide insertion, its reduction into sulfide and the formation of the [2Fe2S] cluster (**Scheme 1**, steps 4 and 5). A number of potential intermediate states of the iron center have been identified here that will help elucidate the mechanism of Fe-S cluster assembly in future studies.

Methods

Chemicals

Sodium phosphate dibasic (Na_2HPO_4), Tris(hydroxymethyl)aminomethane hydrochloride (Tris-HCl), 4-(2-hydroxyethyl)-1-piperazineethanesulfonic acid (HEPES), sodium chloride (NaCl), sodium dodecyl sulfate (SDS), dithiothreitol (DTT), L-cysteine, protease inhibitor cocktail (sigmafast), His_6-thrombin, diethylene triamine pentaacetic acid (DTPA), isopropyl β-D-1-thiogalactopyranoside (IPTG), ferrous ammonium sulfate ($Fe(NH_4)_2(SO_4)_2$), imidazole, zinc sulfate ($ZnSO_4$), β -mercaptoethanol, acrylamide:bis-acrylamide (29:1), Mal-d-PEG, phenylmethylsulfonyl fluoride (PMSF), Ethylenediaminetetraacetic acid (EDTA), pyridoxal phosphate (PLP), ferric ammonium citrate (FAC), riboflavin 5'-monophosphate sodium (riboflavin), ammonium sulfate (NH_4SO_4), low molecular weight size-exclusion calibration kit were from Sigma–Aldrich. HisBind Resin from Novagen, Superdex, Q-sepharose and Phenyl Sepharose columns from GE Healthcare, Amicon Ultra-15 Centrifugal Filter Units from Millipore, PD10 column from Amersham Biosciences.

Protein purification

ISCU. *Mm* and *Hs* ISCU2 proteins (referred to as ISCU in the text) were prepared following previously described procedures.[12] Expression of *Ec* IscU with a polyhistidine tag at the N-terminus was performed using *E. coli* strain C41(DE3) carrying pVP67K plasmid encoding IscU-His8.[76] Expression of *Ec* IscU was induced by addition of 1 mM IPTG at OD_{600nm} = 0.6. After 3 h, cells were harvested and lysed in a French Press in buffer A (25 mM Tris-HCl, 150 mM KCl, 10% glycerol, pH 8.0) supplemented with 1 mM PMSF) containing 20 mM imidazole. Cell debris were removed by centrifugation at 75 000 g for 60 min at 4°C. The supernatant was loaded on a HisBind column beforehand washed with buffer A supplemented with 1 M KCl and equilibrated in buffer A. The proteins were eluted over a linear imidazole gradient from 20 to 500 mM in buffer A. The fractions containing *Ec* IscU were pooled and concentrated by ultrafiltration using Amicon Ultra-15 Centrifugal Filter Units with a cutoff of 10 kDa prior treatment with 100 mM KCN for 1h at 25°C to remove polysulfane modification.[77] KCN was subsequently removed by SEC in buffer B (20 mM Tris-HCl, 20 mM KCl, 10 % glycerol, pH 8.0) using a PD10 column. Final preparations of IscU were aliquoted and stored at - 70°C. Expression of *Ct* Isu1 with a polyhistidine tag at the C-terminus was induced in the *E. coli* strain C41(DE3) carrying pET21d ISU1Ct-His6 plasmid by adding IPTG at a final concentration of 1 mM at OD_{600nm} = 0.6. Cells were harvested, suspended in buffer C1 (25 mM Tris–HCl, 10 % glycerol, 1 mM PMSF, 0.5 M KCl, 0.05 % Triton X- 100, 50 mM imidazole, pH 8.0), and lysed using a French press. Cell debris were removed by centrifugation at 75 000 g for 60 min at 4°C. The supernatant was loaded on HisBind column beforehand washed with buffers C2 (25 mM Tris–HCl, 10 % glycerol, 1 mM PMSF, 1 M KCl, 0.05 % Triton X-100, 50 mM imidazole, pH 8.0) and equilibrated in buffer C3 (25 mM Tris–HCl, 10 % glycerol, 1 mM PMSF, 150 mM KCl, 0.05 % Triton X-100, 50 mM imidazole, pH 8.0). The proteins were eluted over a linear imidazole gradient from 50 to 500 mM in buffer C1. The fractions containing *Ct* Isu1 were

pooled and concentrated. Next *Ct* Isu1 was incubated with 100mM KCN for 1h at 25°C to remove polysulfane modifications. KCN was subsequently removed by SEC in buffer B using a PD10 column. Aliquots were shock frozen in liquid nitrogen and stored at - 70°C until use.

Apo-IscU, Fe-IscU. The ISCU proteins (WT and mutants) were incubated with 50 molar equivalents of DTT and 100 molar equivalents of DTPA for 1 hour to remove zinc and keep the cysteines in their reduced states, then loaded on a HiLoad 16/600 Superdex 75 prep grade column pre-equilibrated with buffer T1 (20 mM Tris, 250 mM NaCl, 10 mM DTT, pH 8.0). The fractions containing the monomeric apo form and the oligomeric forms were concentrated to 1-3 mM by centrifugation on Amicon filter membrane 10 kDa and transferred inside the glove box. The samples were desalted and deoxygenated by SEC on a NAP5 column in deoxygenated buffer T2 (20 mM Tris, 100 mM NaCl, pH 8.0). The samples were further deoxygenated by incubation for 2 h at 10°C in opened cap tubes, then aliquoted and stored with glycerol (10% final concentration) at −80 °C.

For experiments performed in other buffers, the apo-ISCU proteins in T2 buffer were buffer exchanged with buffer P (50 mM phosphate, 100 mM NaCl, pH 8.0), H7 (20 mM HEPES, 300 mM NaCl, pH 7.0) or H8 (20 mM HEPES, 300 mM NaCl, pH 8.0) by SEC on a NAP5 column. For experiments performed at various pH in Tris buffer, apo-ISCU proteins in T2 buffer were incubated with different ratios of buffer T2 and buffer T3 (20 mM Tris, 100 mM NaCl, pH 6.5).

NFS1, IscS. *Mm* and *Hs* NFS1-ISD11-ACP complex containing *Ec* ACP were prepared following previously described procedures.[12] For *Ec* IscS protein, C41(DE3) competent cells (Novagen) transformed by the IscS expression plasmid, pET11aIscS,[78] were used to inoculate 400 mL of LB medium containing 100 μg⁄mL ampicillin. The cells were grown overnight at 37 °C. The inoculum was diluted to OD_{600nm} = 0.1 in 6 L of LB medium containing 100 μg/mL ampicillin. The expression of IscS was induced at OD_{600nm} = 0.6 with 1 mM IPTG. Then the cells were supplemented with 50 μM PLP and 3% ethanol and grown at 20°C overnight.[79] Cells were harvested by centrifugation, then freeze/thawed, and lysed by French press in D1 buffer (50 mM Tris-HCl, 1 mM DTT, 0.5 mM EDTA, pH 8.0) containing 0.4 mM PMSF. Cell debris were removed by centrifugation at 75 000 g for 60 min at 4°C. The supernatant was loaded on a Q-sepharose equilibrated in buffer D1 and then the column was washed with buffer D1 containing 0.4 mM PMSF. The protein was eluted using a linear gradient of 0 to 1 M NaCl in buffer D1. The fractions containing IscS were pooled and concentrated using Amicon Ultra-15 then dialyzed against buffer E (100 mM Tris-HC1, 1 mM DTT, pH 8.0). The protein sample was supplemented with 1 M NH_4SO_4 and applied to a Phenyl Sepharose column. IscS was eluted with a linear gradient from 1 M to zero NH_4SO_4. Yellow fractions containing IscS were concentrated by ultrafiltration and further treated with 100μM PLP. Purified IscS was dialyzed to buffer B and stored in - 70 °C until used.

FDX2, Fdx. *Hs* FDX2 was purified as previously described.[12] For *Ec* Fdx, BL21(DE3) cells transformed with pDEST24Fdx[80] were grown in LB at 37°C and the expression of Fdx was induced with 1 mM IPTG

at OD_{600nm} = 0.6 and supplemented with 50 µM FAC during overnight induction period. Cells were harvested by centrifugation, frozen, thawed, and lysed by French press in F1 buffer (50 mM Tris–HCl, 10 % glycerol, 50 mM NaCl, 2 mM EDTA, pH 7.5) containing 1 mM PMSF. Cell debris were removed by centrifugation at 75 000 g for 60 min at 4°C. The supernatant was loaded on a Q-sepharose column equilibrated in buffer F1 and then the column was washed with buffer F1 containing 1 mM PMSF. Fdx was eluted using a linear gradient of NaCl from 100 mM to 500 mM NaCl in buffer F1. The fractions containing Fdx were pooled and concentrated using Amicon Ultra-15 and then dialyzed against F1 buffer. The samples were then supplemented with 2 M NH_4SO_4 and loaded on a Phenyl Sepharose column. Fdx was eluted with a linear gradient from 2 M to zero NH_4SO_4. Fractions containing Fdx were concentrated by ultrafiltration and dialyzed against buffer F2 (50 mM Tris-HCl, 10 % glycerol, 50 mM NaCl, pH 7.5). The final preparation of Fdx was aliquoted, frozen in liquid nitrogen, and stored at -70°C.

FDXR, FdxR. Expression of human FDXR with a polyhistidine tag was performed in the *E. coli* strain BL21(DE3). Cells were transformed by the FDXR expression plasmid, pETDuet1FDXR and pOFXGroEL plasmid carrying bacterial GroEL to increase the solubility of overproduced FDXR. *E.coli* cells transformed with both plasmids were used to inoculate 400 ml of LB medium containing 100ug/ml ampicillin and 34ug/ml chloramphenicol. The cells were grown overnight at 37 °C. The inoculum was diluted to OD_{600nm} = 0.1 in 6 L of LB medium containing 100 µg/mL ampicillin and 34 ug/mL chloramphenicol. Cells were subsequently grown to OD_{600nm} = 0.6 to induce expression of FDXR by adding IPTG to final concentration of 1 mM. The culture was supplemented with 3.75 µM riboflavin and grown overnight at 25°C. The cells were harvested, suspended in buffer G1 (25mM Tris–HCl, 10% glycerol, 1mM PMSF, 150 mM NaCl, pH 8.0) and lysed using a French press. Cell debris were removed by centrifugation at 75 000 g for 60 min at 4°C. The supernatant was loaded on a HisBind column beforehand washed with buffers G2 (25mM Tris–HCl, 10% glycerol, 1mM PMSF, 500 mM NaCl, 10mM imidazole, pH 8.0) and G3 (25mM Tris–HCl, 10% glycerol, 1mM PMSF, 150mM NaCl, 10mM imidazole, pH 8.0) and equilibrated in buffer G3. The proteins were eluted with a linear gradient imidazole from 10 to 250mM in buffer G1. The fractions containing FDXR were pooled and dialyzed against buffer I1 (25mM Tris–HCl, 50 mM NaCl, 10% glycerol, pH 8.0). The protein sample was loaded to a Q Sepharose column and FDXR was eluted with a linear gradient of NaCl from 50 to 500 mM in buffer I1. Yellow fractions containing FDXR were concentrated by ultrafiltration using Amicon Ultra-15 dialyzed against buffer I1. The preparation of FDXR was aliquoted, frozen in liquid nitrogen, and stored at - 70°C. *Ec* flavodoxin reductase (FdxR) was purified as described with some modifications.[81] HMS174 (DE3) cells containing pET11a-FdxR with N-terminal 6xHis tag were grown overnight in LB medium containing 100 µg/mL ampicillin. 400 mL of the overnight culture were used to inoculate 6 liters of LB medium containing 100 µg/mL ampicillin and the cells were grown at 30 °C. The expression of *Ec* FdxR was induced with 1 mM IPTG at OD_{600nm} = 0.6 and riboflavin was added to a final concentration of 3.75 µM, followed by 4 h of growth/induction. Cells overexpressing FdxR were

pelleted, suspended in ice-cold buffer G3 and lysed by French press. The lysed cells were centrifuged at 75000 g for 60 min. The supernatant was applied to HisBind column equilibrated with buffer G1. The proteins were eluted with a linear gradient of imidazole from 10 to 250 mM in buffer G1. Fractions containing FdxR were pooled and concentrated by ultrafiltration using Amicon Ultra-15 and subjected to buffer exchange to buffer B using a PD10 column. Pure FdxR was aliquoted, frozen in liquid nitrogen, and stored at - 70°C.

Concentration determination

Protein concentrations were determined by electronic absorption spectroscopy at 278 nm in urea 8M, Tris 0.1 M, pH 7.5 using absorption coefficients determined according to Uniprot website with the ProtParam software (see **Supplementary Table 4**).

Size exclusion chromatography

The oligomeric state of the apo-ISCU proteins were determine on Superdex 75 16/600 and Superdex 200 16/600 columns equilibrated in buffer T2 and calibrated using protein standards from high and molecular weight calibration kits (see **Supplementary Fig. S1**). The oligomeric state of iron-loaded H103A mutant was assessed under anaerobic conditions on an analytical Superdex 75 10/300 column equilibrated in buffer T2 and calibrated using a low molecular weight calibration kit.

Redox state of the cysteine residues

The redox state of the cysteine residues in H103A ISCU was probed using a heavy alkylating agent (Mal-dPEG, MW = 2.3 kDa) to generate protein adducts with molecular weights proportional to the number of reduced cysteines that are detected by band shift on SDS-PAGE. A volume of 50 µL of the ISCU H103A protein at a concentration of 20 µM was incubated with 2.3 µL of a solution of Mal-dPEG (3.6 mM in H_2O with 3 % SDS) for 30 min at 20°C. 5 µL of Laemli buffer was added to 9.5 µL of the reaction mixture and incubated for 30 min at 20°C. A volume containing 200 pmoles of ISCU was loaded on 14 % acrylamide gels. The gel was run for 2 hours at 90 V and the proteins were revealed by coomassie staining. The gels were imaged using an Odyssey scanner (Li-COR).

Fe-S cluster assembly assays

Fe-S cluster assembly assays for *Ec*, *Ct*, *Mm* and *Hs* ISCU proteins were performed using a previously described procedure.[12] All the proteins (NFS1, IscS, FDX2, FDXR, Fdx, FdxR, FXN) were buffer exchanged in the glove box on a NAP-5 column with buffer T2 (20 mM Tris, 100 mM NaCl, pH 8.0) then deoxygenated overnight at 10°C and aliquoted with 10 % glycerol, except apo-ISCU proteins that were already prepared and stored under these conditions. The apo *Ec*, *Ct*, *Mm*, *Hs* ISCU proteins (100 µM) were incubated with 1.0 molar equivalent of ferrous iron. Then, *Ec* Fe-IscU (100 µM) was incubated with 5 µM of *Ec* IscS, *Ec* Fdx and *Ec* FdxR, *Mm* and *Ct* Fe-IscU (100 µM) were incubated with 5 µM of *Mm* NFS1-ISD11-ACP, *Hs* FDX2, *Hs* FDXR and *Mm* FXN, and *Hs* Fe-IscU (100 µM)

was incubated with 5 μM of *Hs* NFS1-ISD11-ACP, *Hs* FDX2, *Hs* FDXR and *Mm* FXN. All reactions contained 100 μM of NADPH and 100 μM of L-cysteine and were completed to a final volume of 100 μL with buffer T2. The kinetics of Fe-S cluster assembly were initiated by adding L-cysteine and were monitored at 456 nm by electronic absorption spectroscopy.

For pH studies, the reactions were completed to 100 μL with different ratios of buffer T2 and T3 (20 mM Tris, 100 mM NaCl, pH 6.5). T2:T3 volume ratios of 35:35 μL, 10:60 μL and 0:70 μL were used to reach final pH of 7.7, 7.4 and 7.2.

Electronic absorption and CD spectroscopies

Electronic absorption spectra in the UV-visible domain were acquired using a Secomam UVIKON XL spectrometer and CD spectra using a Jasco J-815 CD spectrometer. For experiments performed in other buffers, the apo-ISCU proteins in T2 buffer were buffer exchanged in buffer P (50 mM phosphate, 100 mM NaCl, pH 8.0), H7 (20 mM HEPES, 300 mM NaCl, pH 7.0) or H8 (20 mM HEPES, 300 mM NaCl, pH 8.0) by SEC on a NAP5 column. Then the proteins (5 μL, 2 mM) were mixed with 5 μL of ferrous ammonium sulfate (2 mM) prepared in water and the solution were completed to 100 μL with the corresponding buffer.

For experiments performed in Tris buffer at various pH, 5 μL of apo-ISCU proteins (2 mM) in T2 buffer were incubated with different ratios of buffer T2 and buffer T3 (20 mM Tris, 100 mM NaCl, pH 6.5). T2:T3 volume ratios of 45:45 μL, 15:75 μL and 8:82 μL were used to reach final pH of 7.7, 7.4 and 7.2. Then the protein samples were mixed with 5 μL of ferrous ammonium sulfate (2 mM) prepared in water.

NMR spectroscopy

$^{15}N^{13}C$ labelled ISCU was produced in minimum medium complemented with 1 $g.L^{-1}$ $^{15}NH_4Cl$, 3 $g.L^{-1}$ ^{13}C-glucose and 20 μM $ZnCl_2$. NMR samples were prepared in 20 mM Tris pH 8.0, 100 mM NaCl buffer. 7.5 % ^2H_2O was added to lock the spectrometer frequency. For Fe-ISCU a valved 3 mm NMR tube was prepared and closed inside the globe box. ^1H-^{15}N SOFAST HMQC spectra (0.2 ms recycling delay, 64 and 256 scans for Zn-ISCU and Fe-ISCU, respectively) were acquired at a temperature of 293 K on a Bruker NMR spectrometer operating at a magnetic field of 18.8 T and equipped with a cryoprobe. Triple resonance experiments for backbone assignment (HNCACB, HBHA(CO)NH and BEST-TROSY versions of HNCO, HNCA, HN(CO)CA, HN(CO)CACB) were carried out for 300 μM Zn-ISCU at 14.1 T at 298K in a buffer supplemented with 1 mM DTT. ^1H chemical shifts were referenced to DSS. NMR data analysis was performed in CCPNMR 2.4 software.[82] The PCS $\Delta\chi$ tensor was fitted using the FANTEN software accessible through the WeNMR portal.[47]

XAS spectroscopy

The Fe-ISCU samples were prepared by incubating monomeric *Mm* apo-ISCU (3 mM) with 0.7 equivalent of ferrous ammonium sulfate salt in Tris buffer containing 20 % of glycerol (final

concentration). The samples were transferred to homemade sample holders and sealed with Kapton tape before freezing in liquid nitrogen. XAS data of model compounds (**1**), (**2**), (**3**) and (**4**) were kindly provided by Serena DeBeer. Synthesis and structural characterizations of compounds (**5**), (**6**) and (**7**) were previously reported.[55,56,58] Crystals of compounds (**5**), (**6**) and (**7**) were crushed into fine powder under anaerobic conditions in a glove box and compacted into pellets using a manual hydraulic press. The samples were mounted on a cannula and inserted into the cryostat. Bulk XAFS analysis of Fe-ISCU and compounds (**5**), (**6**) and (**7**) was conducted at SAMBA beamline, Synchrotron SOLEIL, France. The electron storage ring was operated at 2.75 GeV with a 500 mA beam current. A Si(220) double crystal monochromator was employed, which was calibrated by assigning the first inflection of a Fe foil XANES spectrum to 7112 eV. The XAFS spectra were collected in fluorescence mode using a Ge 33-pixel detector and XIA DxMap DSP cards, XIA cards dead time correction was applied. The sample was cooled to 20K using a He cryostat to reduce thermal disorder and prevent beam damage. Spectra were collected from 7000 to 8000 eV using a continuous scan acquisition mode, with a 1.25 eV/s velocity and 0.16 s/point integration time. Therefore, each scan was obtained in 800 seconds and featured 5000 data points with a 0.2 eV step size. A hundred scans for the protein sample were collected and averaged together to get good S/N ratios. All XAFS data processing (baseline correction, subtraction, normalization, peak integration) were done using Athena and Artemis in Demeter/IFEFFIT software package and the Origin software for peak deconvolution and integration.[83] The pre-edge peaks of the XANES spectra were deconvoluted using the pseudo-Voigt function with 50:50 ratio of Lorentzian and Gaussian functions. A consecutive optimization of amplitudes, band positions and of the half-width of the individual bands was performed in order to obtain the most acceptable fits. The absolute error due to the deconvolution variability and the baseline correction was estimated to be ± 3.5%. No smoothing procedures were applied. EXAFS data were converted to k space using an E_0 value of 7122 eV. The EXAFS data of Fe-ISCU were fitted over a k range of 3 to 12.0 $Å^{-1}$ using a constant amplitude reduction factor, S_o^2= 0.95. The spectra were fitted using the following parameters: *N*, the number of coordinating atoms, σ^2, the Debye–Waller factor and *R*, the distance between the absorber (Fe) and the backscattering atoms. The crystallographic data of the model compound (**3**) (open crystallography database, ID 4302291)[84] were used in IFEFFIT to provide initial values for atomic scattering amplitudes and phase shifts in EXAFS fits. A first fit was performed with all parameters free (Fi t#1) and then several other fits with pre-set number and nature of coordinating atoms (Fit #2 to #9) to evaluate the robustness of the first fit. The goodness of fit was evaluated based on the values of σ^2 ($\sigma^2 < 6.10^{-3}$ $Å^2$) and of the *R*-factor with values < 0.02 denoting that the fit is good enough.[85]

Mössbauer spectroscopy

The C104S and H103A Fe-ISCU mutant samples were prepared by incubating monomeric *Mm* apo-ISCU C104S and H103A (1-2 mM) with 0.5 molar equivalent of ^{57}Fe ammonium sulfate salt to a final volume of 350 μL in Tris buffer containing 10% glycerol. The samples were transferred into homemade

sample holders and freezed inside the glove box. Mössbauer spectra were recorded in the constant acceleration mode with a conventional spectrometer from Wissel GmbH with a multi-channel analyzer in the time-scale mode (WissEL GmbH). LN_2 bath cryostat from Oxford Instruments and WissEl GmbH were used to conduct experiments at 77 K. Isomer shifts δ are given relative to α-iron at room temperature. After transfer of the data from the multi-channel analyzer to a PC the public domain software Vinda[86] running on an Excel 2003 platform was used to analyze the data. Spectra were analyzed by least-squared fits using Lorentzian line shapes.

EPR spectroscopy

The EPR samples were prepared by mixing monomeric *Mm* apo-ISCU WT, C104S and H103A (0.7 – 1 mM) with 0.5 - 0.7 molar equivalents of ferrous ammonium sulfate in either Tris or phosphate buffers containing 10% of glycerol to a final volume of 180 μL. The samples were transferred into calibrated quartz EPR tubes and then sealed with a septum before freezing in liquid nitrogen. EPR spectroscopy experiments were performed on a Bruker Elexsys E500 spectrometer fitted with an Oxford Instruments ESR-900 helium-gas flow for cryogenic temperature studies and mounted with a Bruker dual mode resonator (ER 4116DM). The magnetic properties of the high spin Fe^{II} center of Fe-ISCU were analyzed using the spin Hamiltonian formalism, as described first for $S = 2$ spin system by Abragam and Bleaney and then developed by others.[87,88] Briefly, the Spin Hamiltonian (*H*s) is written as:

$$Hs = D\left(\boldsymbol{S}_z^2 - \left(\frac{1}{3}\right)S(S+1)\right) + E\left(\boldsymbol{S}_x^2 - \boldsymbol{S}_y^2\right) + \beta \boldsymbol{B}\boldsymbol{g}\boldsymbol{S}$$

The first two terms describe the zero-field splitting (ZFS), incorporating the axial (*D*) and rhombic (*E*) parameters at zero field, while the last term describes the Zeeman interaction. For the $S = 2$ Fe^{II} spin system considered here, the zero-field energy (~ *D*) is much larger than the energy of the Zeeman interaction ($h\nu \sim 0.3$ cm^{-1} at X-band). Thus, in the absence of magnetic field, the non-Kramers doublets "$M_S = \pm 2$", "$M_S = \pm 1$" and "$M_S = 0$", which are mixed states of the pure $|M_S|$ states when rhombicity ($E/D \neq 0$) happens, are well separated and their energy simply rely on the ZFS parameters.[88] The Boltzmann distribution of the "$M_S = \pm 2$" sub-level population depends mostly on the *D* term and was then fitted with the convenient assumption of an axial (E=0) zero-field splitting case, for which the energies of the $M_S = \pm 2$, $M_S = \pm 1$ and $M_S = 0$ sub-levels are $+2D$, $-D$ and $-2D$, respectively, thus leading to the equation:

$$N_{\pm 2} = \frac{N}{1 + e^{\frac{3D}{k_B T}} + \frac{1}{2}e^{\frac{4D}{k_B T}}}$$

where $N_{\pm 2}$ and N correspond to the populations of the $M_S = \pm 2$ sub-level and of the $S = 2$ manifold, respectively, k_B is the Boltzmann constant (~ 0.7 cm^{-1}.K). The $N_{\pm 2}$ population is proportional to the

intensity (or the amplitude) of the low-field EPR signal associated to the non-Kramers "$M_S = \pm 2$" doublet over the temperature and can therefore be experimentally estimated.

Numerical simulations were achieved using the Easyspin toolbox assuming a $S = 2$ system and an isotropic $g = 2$ tensor.[89] The line shapes were generated with an explicit loop over Gaussian distribution of the Spin Hamiltonian parameters, either D or E/D. Simulations were cut at low magnetic field because divergence happened at resonance fields approaching zero, depending on numerical sampling and on the magnetic field range that was explored.[62] The Gaussian distribution of the rhombicity parameter E/D used in the spectral simulations was given as FWHM (Full Width at Half Maximum) which is proportional to the standard deviation, σ, through the relation FWHM ~ $2.3548 \times \sigma$.

TOC Graphic

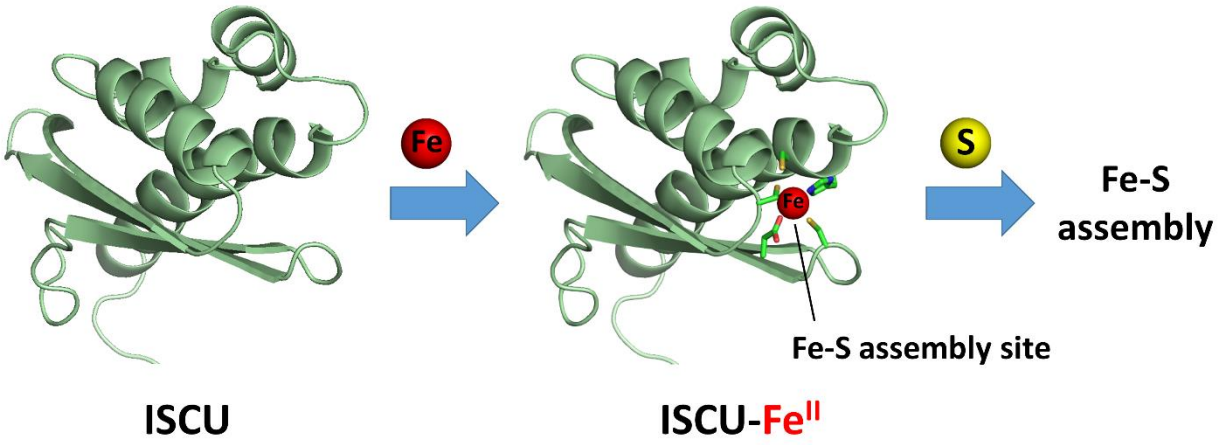

Supporting Information

Figures: Calibration curves of SEC columns, Mössbauer, UV-visible and CD spectra, structures of Fe^{II} model complexes, deconvoluted XANES spectra, EPR temperature dependence studies.

Tables: Elution volumes and molecular weight determined by SEC, Mössbauer parameters, absorption coefficients of the proteins at 280 nm.

Text: determination of the ZFS parameters, analysis of the Mössbauer parameters.

Acknowledgments

This work was funded by the French national research agency (ANR-17-CE11-0021 Frataxur, awarded to B.D.A.), Fondation pour la Recherche Medicale (FDT202012010541, awarded to S.G.), the Polish National Science Center Grant UMO-2015/19/B/NZ1/00237 (to R.D.) and the N.I.H. (R01GM119374 to D.P.G.). V.S. acknowledges support by the DFG (SPP1927) via grant SCHU 1251/17–2. The authors are grateful to SOLEIL for provision of synchrotron radiation facilities and beamline SAMBA, the EPR-MRS facility of the French Research Infrastructure INFRANALYTICS (FR2054) and the Aix-Marseille University EPR center. We are grateful to Serena DeBeer (Max Planck Institute for Chemical Energy Conversion, Mülheim an der Ruhr, Germany) for providing XAS data of compounds 1 - 4.

References

(**1**) Srour, B.; Gervason, S.; Monfort, B.; D'Autréaux, B. Mechanism of Iron-Sulfur Cluster Assembly: In the Intimacy of Iron and Sulfur Encounter. *Inorganics* **2020**, *8*, 55.
(**2**) Garcia, P. S.; Gribaldo, S.; Py, B.; Barras, F. The SUF system: an ABC ATPase-dependent protein complex with a role in Fe-S cluster biogenesis. *Res. Microbiol.* **2019**, *170*, 426-434.
(**3**) Roche, B.; Aussel, L.; Ezraty, B.; Mandin, P.; Py, B.; Barras, F. Iron/sulfur proteins biogenesis in prokaryotes: formation, regulation and diversity. *Biochim. Biophys. Acta* **2013**, *1827*, 455-469.
(**4**) Hu, Y.; Ribbe, M. W. Biosynthesis of the Metalloclusters of Nitrogenases. *Annu. Rev. Biochem.* **2016**, *85*, 455-483.
(**5**) Chahal, H. K.; Boyd, J. M.; Outten, F. W. Iron–Sulfur Cluster Biogenesis in Archaea and Bacteria In *Encyclopedia of Inorganic and Bioinorganic Chemistry*; Scott, R. A., Ed.; John Wiley & Sons, Ltd: **2013**, p 1-27.
(**6**) Boyd, E. S.; Thomas, K. M.; Dai, Y.; Boyd, J. M.; Outten, F. W. Interplay between oxygen and Fe-S cluster biogenesis: insights from the Suf pathway. *Biochemistry* **2014**, *53*, 5834-5847.
(**7**) Lill, R.; Freibert, S. A. Mechanisms of Mitochondrial Iron-Sulfur Protein Biogenesis. *Annu. Rev. Biochem.* **2020**, *89*, 471-499.
(**8**) Przybyla-Toscano, J.; Roland, M.; Gaymard, F.; Couturier, J.; Rouhier, N. Roles and maturation of iron-sulfur proteins in plastids. *J. Biol. Inorg. Chem.* **2018**, *23*, 545-566.
(**9**) Iwasaki, T. Iron-Sulfur World in Aerobic and Hyperthermoacidophilic Archaea Sulfolobus. *Archaea* **2010**, *2010*, 842639.
(**10**) Baussier, C.; Fakroun, S.; Aubert, C.; Dubrac, S.; Mandin, P.; Py, B.; Barras, F. Chapter One - Making iron-sulfur cluster: structure, regulation and evolution of the bacterial ISC system In *Advances in Microbial Physiology*; Poole, R. K., Ed.; Academic Press: **2020**; Vol. 76, p 1-39.
(**11**) Freibert, S. A.; Boniecki, M. T.; Stumpfig, C.; Schulz, V.; Krapoth, N.; Winge, D. R.; Muhlenhoff, U.; Stehling, O.; Cygler, M.; Lill, R. N-terminal tyrosine of ISCU2 triggers [2Fe-2S] cluster synthesis by ISCU2 dimerization. *Nat. Commun.* **2021**, *12*, 6902.
(**12**) Gervason, S.; Larkem, D.; Mansour, A. B.; Botzanowski, T.; Muller, C. S.; Pecqueur, L.; Le Pavec, G.; Delaunay-Moisan, A.; Brun, O.; Agramunt, J.; Grandas, A.; Fontecave, M.; Schunemann, V.; Cianferani, S.; Sizun, C.; Toledano, M. B.; D'Autreaux, B. Physiologically relevant reconstitution of iron-sulfur cluster biosynthesis uncovers persulfide-processing functions of ferredoxin-2 and frataxin. *Nat. Commun.* **2019**, *10*, 3566.
(**13**) Monfort, B.; Want, K.; Gervason, S.; D'Autreaux, B. Recent Advances in the Elucidation of Frataxin Biochemical Function Open Novel Perspectives for the Treatment of Friedreich's Ataxia. *Front. Neurosci.* **2022**, *16*, 838335.
(**14**) Parent, A.; Elduque, X.; Cornu, D.; Belot, L.; Le Caer, J. P.; Grandas, A.; Toledano, M. B.; D'Autreaux, B. Mammalian frataxin directly enhances sulfur transfer of NFS1 persulfide to both ISCU and free thiols. *Nat. Commun.* **2015**, *6*, 5686.
(**15**) Webert, H.; Freibert, S. A.; Gallo, A.; Heidenreich, T.; Linne, U.; Amlacher, S.; Hurt, E.; Muhlenhoff, U.; Banci, L.; Lill, R. Functional reconstitution of mitochondrial Fe/S cluster synthesis on Isu1 reveals the involvement of ferredoxin. *Nat. Commun.* **2014**, *5*, 5013.
(**16**) Johnson, D. C.; Unciuleac, M. C.; Dean, D. R. Controlled expression and functional analysis of iron-sulfur cluster biosynthetic components within Azotobacter vinelandii. *J. Bacteriol.* **2006**, *188*, 7551-61.
(**17**) Yoon, H.; Knight, S. A.; Pandey, A.; Pain, J.; Turkarslan, S.; Pain, D.; Dancis, A. Turning Saccharomyces cerevisiae into a Frataxin-Independent Organism. *PLoS Genet.* **2015**, *11*, e1005135.
(**18**) Garland, S. A.; Hoff, K.; Vickery, L. E.; Culotta, V. C. Saccharomyces cerevisiae ISU1 and ISU2: members of a well-conserved gene family for iron-sulfur cluster assembly. *J. Mol. Biol.* **1999**, *294*, 897-907.

(**19**) Tanaka, N.; Yuda, E.; Fujishiro, T.; Hirabayashi, K.; Wada, K.; Takahashi, Y. Identification of IscU residues critical for de novo iron-sulfur cluster assembly. *Mol. Microbiol.* **2019**, *112*, 1769-1783.
(**20**) Johnson, D. C.; Dean, D. R.; Smith, A. D.; Johnson, M. K. Structure, function and formation of biological iron-sulfur clusters. *Annu. Rev. Biochem.* **2005**, *74*, 247-281.
(**21**) Roche, B.; Agrebi, R.; Huguenot, A.; Ollagnier de Choudens, S.; Barras, F.; Py, B. Turning Escherichia coli into a Frataxin-Dependent Organism. *PLoS Genet.* **2015**, *11*, e1005134.
(**22**) Agar, J. N.; Krebs, C.; Frazzon, J.; Huynh, B. H.; Dean, D. R.; Johnson, M. K. IscU as a scaffold for iron-sulfur cluster biosynthesis: sequential assembly of [2Fe-2S] and [4Fe-4S] clusters in IscU. *Biochemistry* **2000**, *39*, 7856-62.
(**23**) Bonomi, F.; Iametti, S.; Morleo, A.; Ta, D.; Vickery, L. E. Facilitated transfer of IscU-[2Fe2S] clusters by chaperone-mediated ligand exchange. *Biochemistry* **2011**, *50*, 9641-50.
(**24**) Foster, M. W.; Mansy, S. S.; Hwang, J.; Penner-Hahn, J. E.; Surerus, K. K.; Cowan, J. A. A Mutant Human IscU Protein Contains a Stable [2Fe−2S]2+ Center of Possible Functional Significance. *J. Am. Chem. Soc.* **2000**, *122*, 6805-6806.
(**25**) Marinoni, E. N.; de Oliveira, J. S.; Nicolet, Y.; Amara, P.; Dean, D. R.; Fontecilla-Camps, J. C. (IscS-IscU)2 complex structures provide insights into Fe2S2 biogenesis and transfer. *Angew. Chem.* **2012**, *51*, 5439-42.
(**26**) Shimomura, Y.; Wada, K.; Fukuyama, K.; Takahashi, Y. The asymmetric trimeric architecture of [2Fe-2S] IscU: implications for its scaffolding during iron-sulfur cluster biosynthesis. *J. Mol. Biol.* **2008**, *383*, 133-43.
(**27**) Kunichika, K.; Nakamura, R.; Fujishiro, T.; Takahashi, Y. The Structure of the Dimeric State of IscU Harboring Two Adjacent [2Fe-2S] Clusters Provides Mechanistic Insights into Cluster Conversion to [4Fe-4S]. *Biochemistry* **2021**, *60*, 1569-1572.
(**28**) Boniecki, M. T.; Freibert, S. A.; Muhlenhoff, U.; Lill, R.; Cygler, M. Structure and functional dynamics of the mitochondrial Fe/S cluster synthesis complex. *Nat. Commun.* **2017**, *8*, 1287.
(**29**) Fox, N. G.; Yu, X.; Feng, X.; Bailey, H. J.; Martelli, A.; Nabhan, J. F.; Strain-Damerell, C.; Bulawa, C.; Yue, W. W.; Han, S. Structure of the human frataxin-bound iron-sulfur cluster assembly complex provides insight into its activation mechanism. *Nat. Commun.* **2019**, *10*, 2210.
(**30**) Ramelot, T. A.; Cort, J. R.; Goldsmith-Fischman, S.; Kornhaber, G. J.; Xiao, R.; Shastry, R.; Acton, T. B.; Honig, B.; Montelione, G. T.; Kennedy, M. A. Solution NMR structure of the iron-sulfur cluster assembly protein U (IscU) with zinc bound at the active site. *J. Mol. Biol.* **2004**, *344*, 567-83.
(**31**) Iannuzzi, C.; Adrover, M.; Puglisi, R.; Yan, R.; Temussi, P. A.; Pastore, A. The role of zinc in the stability of the marginally stable IscU scaffold protein. *Protein Sci.* **2014**, *23*, 1208-19.
(**32**) Kim, J. H.; Fuzery, A. K.; Tonelli, M.; Ta, D. T.; Westler, W. M.; Vickery, L. E.; Markley, J. L. Structure and dynamics of the iron-sulfur cluster assembly scaffold protein IscU and its interaction with the cochaperone HscB. *Biochemistry* **2009**, *48*, 6062-71.
(**33**) Dzul, S. P.; Rocha, A. G.; Rawat, S.; Kandegedara, A.; Kusowski, A.; Pain, J.; Murari, A.; Pain, D.; Dancis, A.; Stemmler, T. L. In vitro characterization of a novel Isu homologue from Drosophila melanogaster for de novo FeS-cluster formation. *Metallomics* **2017**, *9*, 48-60.
(**34**) Lewis, B. E.; Mason, Z.; Rodrigues, A. V.; Nuth, M.; Dizin, E.; Cowan, J. A.; Stemmler, T. L. Unique roles of iron and zinc binding to the yeast Fe-S cluster scaffold assembly protein "Isu1". *Metallomics* **2019**, *11*, 1820-1835.
(**35**) Rodrigues, A. V.; Kandegedara, A.; Rotondo, J. A.; Dancis, A.; Stemmler, T. L. Iron loading site on the Fe-S cluster assembly scaffold protein is distinct from the active site. *Biometals* **2015**, *28*, 567-76.
(**36**) Lin, C. W.; McCabe, J. W.; Russell, D. H.; Barondeau, D. P. Molecular Mechanism of ISC Iron-Sulfur Cluster Biogenesis Revealed by High-Resolution Native Mass Spectrometry. *J. Am. Chem. Soc.* **2020**, *142*, 6018-6029.
(**37**) Cai, K.; Frederick, R. O.; Kim, J. H.; Reinen, N. M.; Tonelli, M.; Markley, J. L. Human mitochondrial chaperone (mtHSP70) and cysteine desulfurase (NFS1) bind preferentially to the disordered conformation, whereas co-chaperone (HSC20) binds to the structured conformation of the iron-sulfur cluster scaffold protein (ISCU). *J. Biol. Chem.* **2013**, *288*, 28755-70.
(**38**) Spiro, S.; D'Autreaux, B. Non-heme iron sensors of reactive oxygen and nitrogen species. *Antioxid. Redox Signal.* **2012**, *17*, 1264-76.
(**39**) Moura, I.; Tavares, P.; Moura, J. J.; Ravi, N.; Huynh, B. H.; Liu, M. Y.; LeGall, J. Purification and characterization of desulfoferrodoxin. A novel protein from Desulfovibrio desulfuricans (ATCC 27774) and from Desulfovibrio vulgaris (strain Hildenborough) that contains a distorted rubredoxin center and a mononuclear ferrous center. *J. Biol. Chem.* **1990**, *265*, 21596-602.
(**40**) McLaughlin, M. P.; Retegan, M.; Bill, E.; Payne, T. M.; Shafaat, H. S.; Peña, S.; Sudhamsu, J.; Ensign, A. A.; Crane, B. R.; Neese, F.; Holland, P. L. Azurin as a Protein Scaffold for a Low-coordinate Nonheme Iron Site with a Small-molecule Binding Pocket. *J. Am. Chem. Soc.* **2012**, *134*, 19746-19757.
(**41**) Dunham, W. R.; Carroll, R. T.; Thompson, J. F.; Sands, R. H.; Funk, M. O., Jr. The initial characterization of the iron environment in lipoxygenase by Mossbauer spectroscopy. *Eur. J. Biochem.* **1990**, *190*, 611-7.
(**42**) Bill, E.; Haas, C.; Ding, X. Q.; Maret, W.; Winkler, H.; Trautwein, A. X.; Zeppezauer, M. Fe(Ii)-Substituted Horse Liver Alcohol-Dehydrogenase, a Model for Non-Heme Iron Enzymes - Various States of Iron-Dioxygen Interaction Investigated by Mossbauer and Epr Spectroscopy. *Eur. J. Biochem.* **1989**, *180*, 111-121.
(**43**) Jacquamet, L.; Dole, F.; Jeandey, C.; Oddou, J. L.; Perret, E.; Le Pape, L.; Aberdam, D.; Hazemann, J. L.; Michaud-Soret, I.; Latour, J. M. First spectroscopic characterization of Fe-II-Fur, the physiological active form of the Fur protein. *J. Am. Chem. Soc.* **2000**, *122*, 394-395.
(**44**) Schunemann, V.; Meier, C.; Meyer-Klaucke, W.; Winkler, H.; Trautwein, A. X.; Knappskog, P. M.; Toska, K.; Haavik, J. Iron coordination geometry in full-length, truncated, and dehydrated forms of human tyrosine hydroxylase studied by Mossbauer and X-ray absorption spectroscopy. *J. Biol. Chem.* **1999**, *4*, 223-231.

(**45**) Clore, G. M.; Iwahara, J. Theory, Practice, and Applications of Paramagnetic Relaxation Enhancement for the Characterization of Transient Low-Population States of Biological Macromolecules and Their Complexes. *Chem. Rev.* **2009**, *109*, 4108-4139.
(**46**) Otting, G. Protein NMR Using Paramagnetic Ions. *Annu. Rev. Biophys.* **2010**, *39*, 387-405.
(**47**) Rinaldelli, M.; Carlon, A.; Ravera, E.; Parigi, G.; Luchinat, C. FANTEN: a new web-based interface for the analysis of magnetic anisotropy-induced NMR data. *J. Biomol. NMR* **2015**, *61*, 21-34.
(**48**) Chandrasekaran, P.; Chiang, K. P.; Nordlund, D.; Bergmann, U.; Holland, P. L.; DeBeer, S. Sensitivity of X-ray Core Spectroscopy to Changes in Metal Ligation: A Systematic Study of Low-Coordinate, High-Spin Ferrous Complexes. *Inorg. Chem.* **2013**, *52*, 6286-6298.
(**49**) Randall, C. R.; Shu, L.; Chiou, Y.-M.; Hagen, K. S.; Ito, M.; Kitajima, N.; Lachicotte, R. J.; Zang, Y.; Que, L. X-ray Absorption Pre-Edge Studies of High-spin Iron(II) Complexes. *Inorg. Chem.* **1995**, *34*, 1036-1039.
(**50**) Westre, T. E.; Kennepohl, P.; DeWitt, J. G.; Hedman, B.; Hodgson, K. O.; Solomon, E. I. A Multiplet Analysis of Fe K-Edge 1s → 3d Pre-Edge Features of Iron Complexes. *J. Am. Chem. Soc.* **1997**, *119*, 6297-6314.
(**51**) Kowalska, J. K.; Hahn, A. W.; Albers, A.; Schiewer, C. E.; Bjornsson, R.; Lima, F. A.; Meyer, F.; DeBeer, S. X-ray Absorption and Emission Spectroscopic Studies of $[L_2Fe_2S_2](n)$ Model Complexes: Implications for the Experimental Evaluation of Redox States in Iron-Sulfur Clusters. *Inorg. Chem.* **2016**, *55*, 4485-97.
(**52**) Tsai, Y.-F.; Luo, W.-I.; Chang, J.-L.; Chang, C.-W.; Chuang, H.-C.; Ramu, R.; Wei, G.-T.; Zen, J.-M.; Yu, S. S. F. Electrochemical Hydroxylation of C3–C12 n-Alkanes by Recombinant Alkane Hydroxylase (AlkB) and Rubredoxin-2 (AlkG) from Pseudomonas putida GPo1. *Sci. Reports* **2017**, *7*, 8369.
(**53**) Tsai, M. C.; Tsai, F. T.; Lu, T. T.; Tsai, M. L.; Wei, Y. C.; Hsu, I. J.; Lee, J. F.; Liaw, W. F. Relative binding affinity of thiolate, imidazolate, phenoxide, and nitrite toward the $\{Fe(NO)_2\}$ motif of dinitrosyl iron complexes (DNICs): the characteristic pre-edge energy of $\{Fe(NO)_2\}^9$ DNICs. *Inorg. Chem.* **2009**, *48*, 9579-91.
(**54**) Albers, A.; Demeshko, S.; Pröpper, K.; Dechert, S.; Bill, E.; Meyer, F. A Super-Reduced Diferrous [2Fe-2S] Cluster. *J. Am. Chem. Soc.* **2013**, *135*, 1704-1707.
(**55**) Gordon, J. B.; Vilbert, A. C.; DiMucci, I. M.; MacMillan, S. N.; Lancaster, K. M.; Moënne-Loccoz, P.; Goldberg, D. P. Activation of Dioxygen by a Mononuclear Nonheme Iron Complex: Sequential Peroxo, Oxo, and Hydroxo Intermediates. *J. Am. Chem. Soc.* **2019**, *141*, 17533-17547.
(**56**) Komuro, T.; Matsuo, T.; Kawaguchi, H.; Tatsumi, K. Coordination Chemistry of Silanedithiolato Ligands Derived from Cyclotrisilathiane: Synthesis and Structures of Complexes of Iron(II), Cobalt(II), Palladium(II), Copper(I), and Silver(I). *Inorg. Chem.* **2003**, *42*, 5340-5347.
(**57**) McDonald, A. R.; Bukowski, M. R.; Farquhar, E. R.; Jackson, T. A.; Koehntop, K. D.; Seo, M. S.; De Hont, R. F.; Stubna, A.; Halfen, J. A.; Münck, E.; Nam, W.; Que, L. Sulfur versus Iron Oxidation in an Iron−Thiolate Model Complex. *J. Am. Chem. Soc.* **2010**, *132*, 17118-17129.
(**58**) Gordon, J. B.; McGale, J. P.; Prendergast, J. R.; Shirani-Sarmazeh, Z.; Siegler, M. A.; Jameson, G. N. L.; Goldberg, D. P. Structures, Spectroscopic Properties, and Dioxygen Reactivity of 5- and 6-Coordinate Nonheme Iron(II) Complexes: A Combined Enzyme/Model Study of Thiol Dioxygenases. *J. Am. Chem. Soc.* **2018**, *140*, 14807-14822.
(**59**) Randall, C. R.; Zang, Y.; True, A. E.; Que, L.; Charnock, J. M.; Garner, C. D.; Fujishima, Y.; Schofield, C. J.; Baldwin, J. E. X-ray absorption studies of the ferrous active site of isopenicillin N synthase and related model complexes. *Biochemistry* **1993**, *32*, 6664-6673.
(**60**) Scott, R. A.; Wang, S.; Eidsness, M. K.; Kriauciunas, A.; Frolik, C. A.; Chen, V. J. X-ray absorption spectroscopic studies of the high-spin iron(II) active site of isopenicillin N synthase: evidence for iron-sulfur interaction in the enzyme-substrate complex. *Biochemistry* **1992**, *31*, 4596-4601.
(**61**) Hagen, W. R. *Biomolecular EPR Spectroscopy*; 1st ed.; CRC Press: Boca Raton, 2008.
(**62**) Hendrich, M. P.; Debrunner, P. G. Integer-spin electron paramagnetic resonance of iron proteins. *Biophys. J.* **1989**, *56*, 489-506.
(**63**) Harman, W. H.; Harris, T. D.; Freedman, D. E.; Fong, H.; Chang, A.; Rinehart, J. D.; Ozarowski, A.; Sougrati, M. T.; Grandjean, F.; Long, G. J.; Long, J. R.; Chang, C. J. Slow Magnetic Relaxation in a Family of Trigonal Pyramidal Iron(II) Pyrrolide Complexes. *J. Am. Chem. Soc.* **2010**, *132*, 18115-18126.
(**64**) Cremades, E.; Ruiz, E. Mononuclear FeII Single-Molecule Magnets: A Theoretical Approach. *Inorg. Chem.* **2011**, *50*, 4016-4020.
(**65**) Atanasov, M.; Ganyushin, D.; Pantazis, D. A.; Sivalingam, K.; Neese, F. Detailed Ab Initio First-Principles Study of the Magnetic Anisotropy in a Family of Trigonal Pyramidal Iron(II) Pyrrolide Complexes. *Inorg. Chem.* **2011**, *50*, 7460-7477.
(**66**) Mathies, G.; Chatziefthimiou, S. D.; Maganas, D.; Sanakis, Y.; Sottini, S.; Kyritsis, P.; Groenen, E. J. J. High-frequency EPR study of the high-spin FeII complex $Fe[(SPPh_2)_2N]_2$. *J. Mag. Res.* **2012**, *224*, 94-100.
(**67**) Lemercier, G.; Mulliez, E.; Brouca-Cabarrecq, C.; Dahan, F.; Tuchagues, J. P. Iron(II) carboxylate complexes based on a tetraimidazole ligand as models of the photosynthetic non-heme ferrous sites: synthesis, crystal structure, and Mossbauer and magnetic studies. *Inorg. Chem.* **2004**, *43*, 2105-13.
(**68**) Aslamkhan, A. G.; Aslamkhan, A.; Ahearn, G. A. Preparation of metal ion buffers for biological experimentation: A methods approach with emphasis on iron and zinc. *J. Exp. Zoo.* **2002**, *292*, 507-522.
(**69**) Yoshimura, Y.; Matsuzaki, Y.; Watanabe, T.; Uchiyama, K.; Ohsawa, K.; Imaeda, K. Effects of Buffer Solutions and Chelators on the Generation of Hydroxyl Radical and the Lipid Peroxidation in the Fenton Reaction System. *J. Clin. Biochem. Nut.* **1992**, *13*, 147-154.
(**70**) Llopis, J.; McCaffery, J. M.; Miyawaki, A.; Farquhar, M. G.; Tsien, R. Y. Measurement of cytosolic, mitochondrial, and Golgi pH in single living cells with green fluorescent proteins. *Proc. Natl. Acad. Sci.* **1998**, *95*, 6803.

(**71**) Porcelli, A. M.; Ghelli, A.; Zanna, C.; Pinton, P.; Rizzuto, R.; Rugolo, M. pH difference across the outer mitochondrial membrane measured with a green fluorescent protein mutant. *Biochem. Biophys. Res. Commun.* **2005**, *326*, 799-804.
(**72**) Slonczewski, J. L.; Rosen, B. P.; Alger, J. R.; Macnab, R. M. pH homeostasis in Escherichia coli: measurement by 31P nuclear magnetic resonance of methylphosphonate and phosphate. *Proc. Natl. Acad. Sci.* **1981**, *78*, 6271.
(**73**) Hickey, E. W.; Hirshfield, I. N. Low-pH-induced effects on patterns of protein synthesis and on internal pH in Escherichia coli and Salmonella typhimurium. *Appl. Environ. Micro.* **1990**, *56*, 1038-1045.
(**74**) Weitschies, W.; Müller, L.; Grimm, M.; Koziolek, M. Ingestible devices for studying the gastrointestinal physiology and their application in oral biopharmaceutics. *Adv. Drug Deliv. Rev.* **2021**, *176*, 113853.
(**75**) Shin, J.; Jin, Y.-S.; Park, Y.-C.; Park, J.-B.; Lee, Y.-O.; Kim, S.-K.; Kweon, D.-H. Enhancing acid tolerance of Escherichia coli via viroporin-mediated export of protons and its application for efficient whole-cell biotransformation. *Metab. Engineer.* **2021**, *67*, 277-284.
(**76**) Kleczewska, M.; Grabinska, A.; Jelen, M.; Stolarska, M.; Schilke, B.; Marszalek, J.; Craig, E. A.; Dutkiewicz, R. Biochemical Convergence of Mitochondrial Hsp70 System Specialized in Iron-Sulfur Cluster Biogenesis. *Int. J. Mol. Sci.* **2020**, *21*, 3326.
(**77**) Dutkiewicz, R.; Marszalek, J.; Schilke, B.; Craig, E. A.; Lill, R.; Muhlenhoff, U. The Hsp70 chaperone Ssq1p is dispensable for iron-sulfur cluster formation on the scaffold protein Isu1p. *J. Biol. Chem.* **2006**, *281*, 7801-8.
(**78**) Kim, J. H.; Tonelli, M.; Markley, J. L. Disordered form of the scaffold protein IscU is the substrate for iron-sulfur cluster assembly on cysteine desulfurase. *Proc. Natl. Acad. Sci.* **2012**, *109*, 454.
(**79**) Majewska, J.; Ciesielski, S. J.; Schilke, B.; Kominek, J.; Blenska, A.; Delewski, W.; Song, J. Y.; Marszalek, J.; Craig, E. A.; Dutkiewicz, R. Binding of the chaperone Jac1 protein and cysteine desulfurase Nfs1 to the iron-sulfur cluster scaffold Isu protein is mutually exclusive. *J. Biol. Chem.* **2013**, *288*, 29134-42.
(**80**) Kim, J. H.; Frederick, R. O.; Reinen, N. M.; Troupis, A. T.; Markley, J. L. [2Fe-2S]-Ferredoxin Binds Directly to Cysteine Desulfurase and Supplies an Electron for Iron–Sulfur Cluster Assembly but Is Displaced by the Scaffold Protein or Bacterial Frataxin. *J. Am. Chem. Soc.* **2013**, *135*, 8117-8120.
(**81**) Hall, D. A.; Vander Kooi, C. W.; Stasik, C. N.; Stevens, S. Y.; Zuiderweg, E. R. P.; Matthews, R. G. Mapping the interactions between flavodoxin and its physiological partners flavodoxin reductase and cobalamin-dependent methionine synthase. *Proc. Natl. Acad. Sci.* **2001**, *98*, 9521.
(**82**) Vranken, W. F.; Boucher, W.; Stevens, T. J.; Fogh, R. H.; Pajon, A.; Llinas, M.; Ulrich, E. L.; Markley, J. L.; Ionides, J.; Laue, E. D. The CCPN data model for NMR spectroscopy: Development of a software pipeline. *Proteins: Struct., Funct., Bioinfo.* **2005**, *59*, 687-696.
(**83**) Ravel, B.; Newville, M. ATHENA, ARTEMIS, HEPHAESTUS: data analysis for X-ray absorption spectroscopy using IFEFFIT. *J. Synch. Rad.* **2005**, *12*, 537-541.
(**84**) Chiang, K. P.; Barrett, P. M.; Ding, F.; Smith, J. M.; Kingsley, S.; Brennessel, W. W.; Clark, M. M.; Lachicotte, R. J.; Holland, P. L. Ligand dependence of binding to three-coordinate Fe(II) complexes. *Inorg. Chem.* **2009**, *48*, 5106-16.
(**85**) Ibrahim, I. M.; Wu, H.; Ezhov, R.; Kayanja, G. E.; Zakharov, S. D.; Du, Y.; Tao, W. A.; Pushkar, Y.; Cramer, W. A.; Puthiyaveetil, S. An evolutionarily conserved iron-sulfur cluster underlies redox sensory function of the Chloroplast Sensor Kinase. *Commun. Biol.* **2020**, *3*, 13.
(**86**) Gunnlaugsson, H. P. Spreadsheet based analysis of Mössbauer spectra. *Hyperfine Interact* **2016**, *237*, 79.
(**87**) Abragam, A.; Bleaney, B. *Electron Paramagnetic Resonance of Transition Ions*; Oxford University Press: Clarendon Press: Oxford, 1970.
(**88**) Hagen, W. EPR of non-kramers doublets in biological systems: Characterization of an S = 2 system in oxidized cytochrome c oxidase. *Biochim. Biophys. Acta* **1982**, *708*, 82-98.
(**89**) Stoll, S.; Schweiger, A. EasySpin, a comprehensive software package for spectral simulation and analysis in EPR. *J. Mag. Res.* **2006**, *178*, 42-55.